Available online at www.sciencedirect.com
SCIENCE DIRECT
Journal of Sound and Vibration 297 (2006) 17–36
JOURNAL OF SOUND AND VIBRATION
www.elsevier.com/locate/jsvi

Dynamical behavior of a class of vibratory systems with symmetrical rigid stops near the point of codimension two bifurcation

G.W. Luo[a,b,*], Y.L. Zhang[b], J.G. Zhang[a]

[a]School of Mathematics, Physics and Software Engineering, Lanzhou Jiaotong University, Lanzhou, 730070, People's Republic of China
[b]School of Mechanical Engineering, Lanzhou Jiaotong University, Lanzhou 730070, People's Republic of China

Received 28 February 2004; received in revised form 13 February 2006; accepted 16 February 2006
Available online 7 July 2006

Abstract

A multi-degree-of-freedom vibratory system having symmetrically placed rigid stops is considered. The system consists of linear components, but the maximum displacement of one of the masses is limited to a threshold value by the symmetrical rigid stops. Repeated impacts usually occur in the vibratory system due to the rigid amplitude constraints. Such models play an important role in the studies of mechanical systems with clearances or gaps. Local codimension two bifurcation of maps, involving a real eigenvalue and a complex conjugate pair escaping the unit circle simultaneously, is analyzed by using the center manifold theorem technique and normal form method for maps. Symmetrical double-impact periodic motion and Poincaré map of the system are derived analytically. A center manifold theorem technique is applied to reduce the Poincaré map to a three-dimensional one, and the normal form map associated with the codimension two bifurcation is obtained. Local behaviors of the vibratory systems with symmetrical rigid stops, near the points of codimension two bifurcations, are reported by the presentation of results for a two-degree-of-freedom vibratory system with symmetrical stops. The existence and stability of symmetrical double-impact periodic motion are analyzed explicitly. Also, local bifurcations at the points of change in stability, are analyzed. Near the point of codimension two bifurcation, there exists not only Hopf bifurcation of period-one double-impact motion, but also pitchfork bifurcation of the motion. Pitchfork bifurcation of period-one double-impact symmetrical motion results in the period-one double-impact unsymmetrical motion. The unsymmetrical double-impact motion is of two antisymmetrical forms due to different initial conditions and symmetrical stops. With change of the forcing frequency, the unsymmetrical double-impact periodic motion will undergo Hopf bifurcation. Moreover the period-one double-impact symmetrical motion will undergo Hopf bifurcation directly as the forcing frequency is changed in the contrary direction. The routes of quasi-periodic impact motions to chaos are observed by results from simulation.

*Corresponding author. School of Mathematics, Physics and Software Engineering, Lanzhou Jiaotong University, Lanzhou 730070, People's Republic of China.
E-mail addresses: luogw@mail.lzjtu.cn, luogw@hotmail.com (G.W. Luo).

0022-460X/$ - see front matter © 2006 Elsevier Ltd. All rights reserved.
doi:10.1016/j.jsv.2006.02.027

1. Introduction

Vibrating systems with clearances, gaps or stops are frequently encountered in technical applications of mechanism, vehicle traffic and nuclear reactor, etc. Repeated impacts, i.e., vibro-impacts, usually occur whenever the components of a vibrating system collide with rigid obstacles or with each other. The principle of operation of vibration hammers, impact dampers, shakers, pile drivers, offshore structures, machinery for compacting, milling and forming, etc., is based on the impact action for moving bodies. With other equipment, e.g., mechanisms with clearances or gaps, heat exchangers, fuel elements of nuclear reactors, gears, piping systems, wheel–rail interaction of high speed railway coaches, etc., impacts also occur, but they are undesirable as they bring about failures, strain, shorter service life and increased noise levels. Researches into vibro-impact problems have important significance on optimization design of machinery with clearances or stops, noise suppression and reliability analysis, etc. The physical process during impacts is strongly nonlinear and discontinuous, but it can be described theoretically and numerically by discontinuities in good agreement with reality. Compared with single impact, vibro-impact dynamics is more complicated, and hence, has received great attention. Many new problems of theory have been advanced in researches into vibro-impact dynamics, and the study of vibro-impact problems becomes a new subject on nonlinear dynamics. Some important problems on vibro-impact dynamics, including global bifurcations [1–10], grazing singularities [10–18], chattering and rattling impacts [19], quasi-periodic impacts [20–24] and controlling chaos [25,26], etc., have been studied in the past several years. Along with the theory researches into vibro-impact dynamics, the researches into application to these systems were also developed, e.g., wheel–rail impact of railway coaches [27–29], impact noise analysis [30,31], inertial shakers [32,33], vibrating hammer [34], offshore structure [35], impact dampers [36–39] and gears [40–42], etc. However, these studies focused mainly attention on stability and codimension-one bifurcations of periodic-impact motions, codimension two bifurcations of the vibro-impact systems are rarely considered until now.

The purpose of the present study is to focus attention on codimension two bifurcation of period-one double-impact symmetrical motion of vibratory system having symmetrically placed rigid stops. There are many types of codimension two bifurcations of ordinary differential equations and maps, some of which have been studied in Refs. [43–48]. Here one of codimension two bifurcations of maps, involving a real eigenvalue and a complex conjugate pair escaping the unit circle simultaneously, is analyzed by using the center manifold theorem technique and normal form method of maps. A multi-degree-of-freedom systems having symmetrically placed rigid stops and subjected to periodic excitation is considered. The symmetrical double-impact periodic motion and Poincaré map of the system are derived analytically. A center manifold theorem technique is applied to reduce the Poincaré map to a three-dimensional one, and the normal form map associated with the codimension two bifurcation is obtained. The existence and stability of period-one double-impact symmetrical motion are analyzed explicitly. Also, local bifurcations at the points of change in stability, are analyzed. Near the point of codimension two bifurcation there exists not only Hopf bifurcation of period-one double-impact motion, but also pitchfork bifurcation of the motion. Pitchfork bifurcation of symmetrical double-impact periodic motion results in unsymmetrical double-impact periodic motion. With change of the forcing frequency, the unsymmetrical double-impact periodic motion will undergo Hopf bifurcation. Moreover the period-one double-impact symmetrical motion will undergo Hopf bifurcation directly as the forcing frequency is changed in the contrary direction.

2. Mechanical model

A multi-degree-of-freedom system having symmetrically placed rigid stops and subjected to periodic excitation is shown in Fig. 1. Displacements of the masses $M_1, M_2, \ldots, M_{n-1}$ and M_n are represented by $X_1, X_2, \ldots, X_{n-1}$ and X_n, respectively. The masses are connected to linear springs with stiffnesses $K_1, K_2, \ldots, K_{n-1}$ and K_n, and linear viscous dashpots with damping constants $C_1, C_2, \ldots, C_{n-1}$ and C_n. Damping in the mechanical model is assumed as proportional damping. The excitations on the masses are harmonic with amplitudes $P_1, P_2, \ldots, P_{n-1}$ and P_n. The excitation frequency Ω and phase angle τ are the same for these masses. The masses move only in the horizontal direction. For small forcing amplitudes the system will undergo simple oscillations and behave as a linear system. As the amplitude is increased, the kth mass M_k eventually begins to hit the rigid stops and the motion becomes nonlinear (the other masses are not allowed to

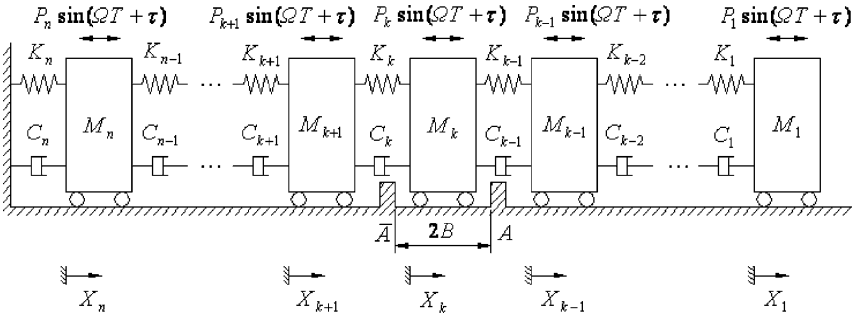

Fig. 1. Schematic of a multi-degree-of-freedom vibratory system with symmetrical rigid stops.

impact any rigid stop). The impact is described by a coefficient of restitution R, and it is assumed that the duration of impact is negligible compared to the period of the force.

Suppose $M_1 \neq 0$, $K_1 \neq 0$, and let $F_0 = |P_1| + |P_2| + \cdots + |P_k| + \cdots + |P_n|$. The non-dimensional quantities are given by

$$m_i = \frac{M_i}{M_1}, \quad k_i = \frac{K_i}{K_1}, \quad f_{i0} = \frac{P_i}{F_0}, \quad \zeta_i = \frac{C_i}{2\sqrt{K_1 M_1}}, \quad x_i = \frac{X_i K_1}{F_0},$$
$$\omega = \Omega\sqrt{\frac{M_1}{K_1}}, \quad t = T\sqrt{\frac{K_1}{M_1}}, \quad \delta = \frac{BK_1}{F_0}, \quad i = 1, 2, \ldots, k, \ldots, n. \tag{1}$$

The motion processes of the system, between consecutive impacts occurring at the stop A, are considered. Between any two consecutive impacts, the time T is always set to zero directly at the starting point A (the mass M_k departing from the $X_k = B$ stop with negative velocity), and the phase angle τ is used only to make a suitable choice for the origin of time in the calculation. The state of the vibro-impact system, immediately after impact, has become new initial conditions in the subsequent process of the motion. Between the stops, the non-dimensional differential equations of motion are given by

$$M\ddot{x} + C\dot{x} + Kx = F\sin(\omega t + \tau), \quad (|x_k| < \delta), \tag{2}$$

where a dot $(\cdot)$ denotes differentiation with respect to the non-dimensional time t; M, K and C are the non-dimensional mass, stiffness and damping matrixes, respectively, $x = (x_1, x_2, \ldots, x_n)^{\mathrm{T}}$, $F = (f_{10}, f_{20}, \ldots, f_{n0})^{\mathrm{T}}$.

Analyzing some special bifurcations of periodic-impact motion of the vibro-impact systems, e.g., strong resonance bifurcations, codimension two bifurcation, etc., one must first find the total-analytical expressions for the periodic-impact motion, Poincaré mapping and associated Jacobian matrix, then compute the exact bifurcation values by using the Jacobian matrix. However, it is difficult that the multi-degree-of-freedom vibro-impact systems with general damping are uncoupled by using a modal matrix approach. In some available references, e.g., Refs. [5–7,23,24], special bifurcations of the vibro-impact systems are studied by assuming such system possessing proportional damping to uncouple the vibration equation and find the total-analytical expressions for the periodic-impact motion, Poincaré mapping and associated Jacobian matrix. In the paper, we adopt the way used in aforementioned references and assume the system possess the proportional damping to find the total-analytical expressions for period-one double-impact symmetric motion, i.e., the damping matrix C, in Eq. (2), is assumed to be the proportional damping matrix (Ref. [49]), $C = \gamma_0 M + \gamma_1 K$. The purpose of the present study is to focus attention on existence of codimension two bifurcations of period-one double-impact symmetrical motion of vibratory system with symmetrical stops. If codimension two bifurcations of period one double-impact symmetric motion are found to exist in the vibro-impact system possessing the proportional damping, it is certain that there exist also corresponding codimension two bifurcations in the vibro-impact system possessing general linear damping.

When the impacts occur, for $|x_k| = \delta$, the velocities of the impacting mass M_k are changed according to the impact law

$$\dot{x}_{kA+} = -R\dot{x}_{kA-} \quad (x_k = \delta), \quad \dot{x}_{k\bar{A}+} = -R\dot{x}_{k\bar{A}-} \quad (x_k = -\delta), \tag{3}$$

where $\dot{x}_{kA-}$ and $\dot{x}_{kA+}$ ($\dot{x}_{k\bar{A}-}$ and $\dot{x}_{k\bar{A}+}$) represent the impacting mass velocities of approach and departure at the instant of impacting with the stop A ($\bar{A}$), respectively.

Let Ψ represent the canonical modal matrix of Eq. (2), $\omega_i (i = 1, 2, \ldots, n)$ denote the eigenfrequiencies of the system, modal damping ratio η_i, damping eigenfrequency $\omega_{di} = \omega_i\sqrt{1-\eta_i^2}$. Eq. (2) is amenable to analytical treatment due to the proportional damping. Using the formal coordinate and modal matrix approach, one can obtain the general solutions of Eq. (2):

$$x(t) = \Psi\xi(t), \tag{4}$$

$$\xi(t) = G(t)A_1 + H(t)B_1 + F_s\sin(\omega t + \tau) + F_c\cos(\omega t + \tau), \quad 0 \leqslant t \leqslant t_1, \tag{5}$$

$$\xi(t) = G(t - t_1)A_2 + H(t - t_1)B_2 + F_s\sin(\omega t + \tau) + F_c\cos(\omega t + \tau), \quad t_1 < t \leqslant t_1 + t_2, \tag{6}$$

in which, it takes the time t_1 and t_2 for the mass M_k to move from the stop A to $\bar{A}$ and from the constraint $\bar{A}$ to A, respectively; A_1, A_2, B_1 and B_2 are the constant matrixes of integration, $G(t) = \mathrm{diag}[e^{-\eta_i\omega_i t}\sin(\omega_{di}t)]$, $H(t) = \mathrm{diag}[e^{-\eta_i\omega_i t}\cos(\omega_{di}t)]$, $i = 1, 2, \ldots, n$ (the symbol "diag[ ]" is used to denote the diagonal matrix); $F_s = \left(f_{s1}, f_{s2}, \ldots, f_{sn}\right)^{\mathrm{T}}$ and $F_c = \left(f_{c1}, f_{c2}, \ldots, f_{cn}\right)^{\mathrm{T}}$ are the amplitude constant vectors.

3. Period-one double-impact symmetrical motion

Periodic-impact motions of the vibratory system with symmetrical rigid stops can be characterized by the symbol n–p–q, where q and p is the number of impacts occurring, respectively, at the constraint A and $\bar{A}$, and n is the number of the forcing cycles. In this section, only the periodic motion of the model, with two symmetrical impacts per force cycle, is considered, which is called period-one double-impact symmetrical motion. Let us choose the Poincaré section $\sigma = \{(x_1, \dot{x}_1, x_2, \dot{x}_2, \ldots, x_k, \dot{x}_k, \ldots, x_n, \dot{x}_n, \theta) \in \mathbf{R}^{2n} \times \mathbf{S}, x_k = \delta, \dot{x}_k = \dot{x}_{k+}\}$ to establish the Poincaré map of the vibratory system with symmetrical rigid stops. The disturbed map of period-one double-impact symmetrical motion is represented briefly by

$$X' = \tilde{f}(v, X), \tag{7}$$

where $\theta = \omega t$, $X \in \mathbf{R}^{2n}$, v is real parameter, $v \in \mathbf{R}^1$ or $\mathbf{R}^2$; $X = X^* + \Delta X$, $X' = X^* + \Delta X'$. $X^* = (x_{10}, x_{20}, \ldots, x_{(k-1)0}, \tau_0, x_{(k+1)0}, \ldots, x_{n0}, \dot{x}_{10}, \dot{x}_{20}, \ldots, \dot{x}_{(k-1)0}, \dot{x}_{k+}, \dot{x}_{(k+1)0}, \ldots, \dot{x}_{n0})^{\mathrm{T}}$ is a fixed point in the hyperplane σ, of which the disturbed vectors are represented by

$$\Delta X = (\Delta x_1, \Delta x_2, \ldots, \Delta x_{k-1}, \Delta\tau, \Delta x_{k+1}, \ldots, \Delta x_n, \Delta\dot{x}_1, \Delta\dot{x}_2, \ldots, \Delta\dot{x}_{k-1}, \Delta\dot{x}_{k+}, \Delta\dot{x}_{k+1}, \ldots, \Delta\dot{x}_n)^{\mathrm{T}},$$

$$\Delta X' = (\Delta x'_1, \Delta x'_2, \ldots, \Delta x'_{k-1}, \Delta\tau', \Delta x'_{k+1}, \ldots, \Delta x'_n, \Delta\dot{x}'_1, \Delta\dot{x}'_2, \ldots, \Delta\dot{x}'_{k-1}, \Delta\dot{x}'_{k+}, \Delta\dot{x}'_{k+1}, \ldots, \Delta\dot{x}'_n)^{\mathrm{T}}.$$

The period-one double-impact symmetrical motion means that if the dimensionless time t is set to zero directly after an impact occurring at the constraint A, it becomes $2\pi/\omega$ just before the next impact occurring at the same constraint. After the origin of θ-coordinate is displaced to an impact point o_1, the determination of period-one double-impact symmetrical motion is based on the fact that they satisfy the following set of periodicity and matching conditions:

$$\begin{bmatrix} x(0) \\ \dot{x}(0) \end{bmatrix} = -\begin{bmatrix} x(\pi/\omega)_+ \\ \dot{x}(\pi/\omega)_+ \end{bmatrix} = D\begin{bmatrix} x(2\pi/\omega) \\ \dot{x}(2\pi/\omega) \end{bmatrix} = \begin{bmatrix} x_0 \\ \dot{x}_0 \end{bmatrix}, \quad \begin{bmatrix} x(\pi/\omega)_- \\ \dot{x}(\pi/\omega)_- \end{bmatrix} = -\begin{bmatrix} x(2\pi/\omega) \\ \dot{x}(2\pi/\omega) \end{bmatrix}, \tag{8}$$

where $D = \mathrm{diag}[d_i]$, $(d_i = 1, i = 1, 2, \ldots, k, \ldots, n + k - 1, n + k + 1, \ldots, 2n; d_{n+k} = -R)$, $x_0 = (x_{10}, x_{20}, \ldots, x_{(k-1)0}, \delta, x_{(k+1)0}, \ldots, x_{n0})^{\mathrm{T}}$, $\dot{x}_0 = (\dot{x}_{10}, \dot{x}_{20}, \ldots, \dot{x}_{(k-1)0}, \dot{x}_{k+}, \dot{x}_{(k+1)0}, \ldots, \dot{x}_{n0})^{\mathrm{T}}$.

The response of 1–1–1 symmetrical orbit is given by

$$\begin{bmatrix} x(t) \\ \dot{x}(t) \end{bmatrix} = \Phi P_1(t)\Phi^{-1}\begin{bmatrix} x(0) \\ \dot{x}(0) \end{bmatrix} + Q_1(t)\begin{bmatrix} \sin\tau \\ \cos\tau \end{bmatrix}, \quad 0 \leqslant t \leqslant \bar{t}_{1-}, \tag{9}$$

$$\begin{bmatrix} x(t) \\ \dot{x}(t) \end{bmatrix} = \Phi P_2(t)\Phi^{-1}D^{-1}\begin{bmatrix} x(0) \\ \dot{x}(0) \end{bmatrix} + Q_2(t)\begin{bmatrix} \sin\tau \\ \cos\tau \end{bmatrix}, \quad \bar{t}_{1+} \leqslant t \leqslant \bar{t}_1 + \bar{t}_2, \tag{10}$$

where $\bar{t}_1 = \bar{t}_2$ and $\bar{t}_1 + \bar{t}_2 = 2\pi/\omega$.

Substituting the formula (8) and inserting $t = 2\pi/\omega$ to the formula (10), one obtains the following equation:

$$\begin{bmatrix} x(0) \\ \dot{x}(0) \end{bmatrix} = D[L - \Phi P_2(2\pi/\omega)\Phi^{-1}]^{-1}Q_2(2\pi/\omega)\begin{bmatrix} S_\tau \\ C_\tau \end{bmatrix}, \tag{11}$$

where L is a unit matrix of degree $2n \times 2n$.

Let $E = D[L - \Phi P_2(2\pi/\omega)\Phi^{-1}]^{-1}Q_2(2\pi/\omega)$, then $E = [e_{ij}]$ is a matrix of degree $2n \times 2$. According to the periodicity and matching conditions (8), one obtains the kth component $x_0(0)$ from the formula (11), which is now

$$x_k(0) = \delta = e_{k1}\sin\tau_0 + e_{k2}\cos\tau_0. \tag{12}$$

Solving Eq. (12) for τ_0 and substituting it for τ in solutions (9) and (10), we obtain the analytical expression for period-one double-impact symmetrical orbit.

4. Disturbed map of period-one double-impact symmetrical motion

If 1–1–1 symmetrical motion is disturbed at the instant of impact by the difference ΔX, then one can express the differences $\Delta X'$ at the instant of the next impact. Between two consecutive impacts occurring at the stop A, the disturbed solutions of 1–1–1 symmetrical motion are written in the form

$$\begin{bmatrix} \tilde{x}(t) \\ \dot{\tilde{x}}(t) \end{bmatrix} = \Phi\tilde{E}(t)\begin{bmatrix} \tilde{A}_1 \\ \tilde{B}_1 \end{bmatrix} + \Phi U\tilde{Q}\begin{bmatrix} \tilde{S}_t \\ \tilde{C}_t \end{bmatrix}, \quad 0 \leqslant t \leqslant \tilde{t}_{1-}, \tag{13}$$

$$\begin{bmatrix} \tilde{x}(t) \\ \dot{\tilde{x}}(t) \end{bmatrix} = \Phi\tilde{E}(t-\tilde{t}_1)\begin{bmatrix} \tilde{A}_2 \\ \tilde{B}_2 \end{bmatrix} + \Phi U\tilde{Q}\begin{bmatrix} \tilde{S}_t \\ \tilde{C}_t \end{bmatrix}, \quad \tilde{t}_{1+} \leqslant t \leqslant t_e, \tag{14}$$

where $\tilde{S}_t = \sin(\omega t + \tau_0 + \Delta\tau)$, $\tilde{C}_t = \cos(\omega t + \tau_0 + \Delta\tau)$, $\tilde{t}_1 = \pi/\omega + \Delta t_1$, $\tilde{t}_2 = \pi/\omega + \Delta t_2$, $t_e = \tilde{t}_1 + \tilde{t}_2$, $\tilde{E}(t) = \begin{bmatrix} G(t) & H(t) \\ \dot{G}(t) & \dot{H}(t) \end{bmatrix}$, $\tilde{Q} = \begin{bmatrix} F_s & F_c \\ -F_c & F_s \end{bmatrix}$, $U = \begin{bmatrix} I & \\ & \omega I \end{bmatrix}$, I is a unit matrix of degree $n \times n$.

For $t = t_e$, Eq. (14) is written by

$$\tilde{Y}_0 = \begin{bmatrix} x_0 + \Delta x' \\ \dot{x}_0 + \Delta\dot{x}' \end{bmatrix} = D\Phi\tilde{E}(\pi/\omega + \Delta t_2)\begin{bmatrix} \tilde{A}_2 \\ \tilde{B}_2 \end{bmatrix} + D\Phi U\tilde{Q}\begin{bmatrix} \tilde{S}_{\Delta t} \\ \tilde{C}_{\Delta t} \end{bmatrix}. \tag{15}$$

where $\tilde{S}_{\Delta t} = \sin(\omega\Delta t_1 + \omega\Delta t_2 + \tau_0 + \Delta\tau)$, $\tilde{C}_{\Delta t} = \cos(\omega\Delta t_1 + \omega\Delta t_2 + \tau_0 + \Delta\tau)$.

Taking $t = \tilde{t}_1$ and t_e, respectively, one obtains, from the kth term of the disturbed solutions (13) and (14), the following formulae:

$$h(\Delta X, \Delta t_1) = \tilde{x}_k(\pi/\omega + \Delta t_1) + \delta = 0, \quad g(\Delta X, \Delta t_1, \Delta t_2) = \tilde{x}_k(2\pi/\omega + \Delta t_1 + \Delta t_2) - \delta = 0. \tag{16}$$

Using the implicit function theorem and supposing $(\partial h/\partial\Delta t_1)\big|_{\Delta X=0} \neq 0$ and $(\partial g/\partial\Delta t_2)\big|_{\Delta X=0} \neq 0$, one can solve Eq. (16) for Δt_1 and Δt_2. Inserting Δt_1 and Δt_2 into the state vector (15), one gets finally the disturbed map of period-one double-impact symmetrical motion

$$\Delta X' = D_1\tilde{Y}_0 + D_2 - X^* \stackrel{\text{Def}}{=} f(v, \Delta X), \tag{17}$$

in which, $D_1 = \text{diag}[d_i^{(1)}]$, $d_i^{(1)} = 1, i = 1, \ldots, k-1, k+1, \ldots, 2n$, $d_k^{(1)} = 0$; $D_2 = \text{diag}[d_i^{(2)}]$, $d_i^{(2)} = 0, i = 1, \ldots, k-1, k+1, \ldots, 2n$, $d_k^{(2)} = \tau'$, $\tau' = \tau_0 + \omega\Delta t_1 + \omega\Delta t_2$.

Linearizing the Poincaré map at the fixed point X^* results in the matrix $\mathrm{D}f(v,0) = \partial f(v, \Delta X)/\partial\Delta X\big|_{(v,\Delta X=0)}$. The stability of 1–1–1 symmetrical motion is determined by computing and analyzing eigenvalues of $\mathrm{D}f(v,0)$.

Variations of the parameters of the system will cause the fixed point and its associated eigenvalues to move. If one of them passes through the unit circle in the complex plane, i.e., $|\lambda_i(v_c) = 1|$ (v_c is a bifurcation value), an instability and an associated bifurcation will occur. In general, bifurcation occurs in various ways according to the numbers of the eigenvalues on the unit circle and their position on the unit circle. Here, we shall consider the case of $v \in \mathbf{R}^2$, and dynamics of the system is studied with special attention to the interaction of Hopf and pitchfork bifurcations of fixed points.

5. Codimension two bifurcation

5.1. The center manifold and normal form map

We continue to consider the map $X' = \tilde{f}(v, X)$. X^* is a fixed point for the map for v in some neighborhood of a critical value $v = v_c$ at which Jacobian matrix $Df(v, 0)$ satisfies the following assumptions:

H.1. Jacobian matrix $Df(v, 0)$ has the eigenvalues $\lambda_1(v_c)$, $\lambda_2(v_c)$ and $\lambda_3(v_c)$ on the unit circle, in which $\lambda_1(v_c)$ is a real eigenvalue and $\lambda_{2,3}(v_c)$ are a pair of complex conjugate eigenvalues, and $\lambda_1(v_c) = 1$, $\lambda_2(v_c) = \bar{\lambda}_3(v_c)$, $|\lambda_{2,3}(v_c)| = 1$.

H.2. The remainder of the spectrum of $Df(v, 0)$ are strictly inside the unit circle.

Let $r_i(v)$ denote the eigenvector of Jacobian matrix $Df(v, 0)$ corresponding to the eigenvalue $\lambda_i(v)$ $(i = 1, 2, \ldots, 2n)$. If $\lambda_j(v)$ is one of a pair complex conjugate eigenvalues ($j \neq 1,2,3$, but j may be $4, \ldots, 2n-1$), the eigenmatrix is expressed by $P = (r_1, \mathrm{Re}\, r_2, -\mathrm{Im}\, r_2, \ldots, \mathrm{Re}\, r_j, -\mathrm{Im}\, r_j, \ldots)$. If $\lambda_j(v)$ is a real eigenvalue ($j \neq 1,2,3$, but j may be $4, 5, \ldots, 2n$), then $P = (r_1, \mathrm{Re}\, r_2, -\mathrm{Im}\, r_2, \ldots, r_j, \ldots)$. For all v in some neighborhood of v_c, the map (17), under the change of variables $\mu_1 = v_1 - v_{1c}$, $\mu_2 = v_2 - v_{2c}$, $\mu = (\mu_1, \mu_2)^{\mathrm{T}}$ and $\Delta X = P\tilde{Y}$, becomes

$$\tilde{Y}' = \tilde{F}(\mu; \tilde{Y}), \tag{18}$$

where $D\tilde{F}(\mu, 0)$ has the form

$$D\tilde{F}(\mu, 0) = \begin{bmatrix} \lambda_1 & 0 & 0 & 0 \\ 0 & \mathrm{Re}\,\lambda_2 & -\mathrm{Im}\,\lambda_2 & 0 \\ 0 & \mathrm{Im}\,\lambda_2 & \mathrm{Re}\,\lambda_2 & 0 \\ 0 & 0 & 0 & \tilde{D}_1 \end{bmatrix}, \tag{19}$$

where $\lambda_i = \tilde{\lambda}_i(\mu) = \lambda_i(v_c + \mu)$, $\tilde{\lambda}_1(0) = 1$, $\tilde{\lambda}_{2,3}(0) = \alpha \pm \mathrm{i}\varpi$, $|\tilde{\lambda}_{2,3}(0)| = 1$. $\tilde{D}_1$ is a real matrix of degree $(2n\text{-}3) \times (2n\text{-}3)$ with the eigenvalues $\tilde{\lambda}_4(\mu), \ldots, \tilde{\lambda}_{2n-1}(\mu)$ and $\tilde{\lambda}_{2n}(\mu)$.

Let $z_1 = y_1$, $z_2 = y_2 + \mathrm{i}y_3$, $\bar{z}_2 = y_2 - \mathrm{i}y_3$, $z = (z_1, z_2, \bar{z}_2)^{\mathrm{T}}$, $G^{(1)} = \tilde{F}_1 - \lambda_1 z_1$, $G^{(2)} = \tilde{F}_2 + \mathrm{i}\tilde{F}_3 - \lambda_2 z_2$, $W = (\tilde{y}_4, \tilde{y}_5, \ldots\ldots, \tilde{y}_{2n})^{\mathrm{T}}$, $H = (\tilde{F}_4, \tilde{F}_5, \ldots\ldots, \tilde{F}_{2n})^{\mathrm{T}} - \tilde{D}_1 W$, the map (18) is rewritten by

$$z_1' = \lambda_1 z_1 + G^{(1)}(z_1, z_2, \bar{z}_2, W; \mu), \quad z_2' = \lambda_2 z_2 + G^{(2)}(z_1, z_2, \bar{z}_2, W; \mu),$$

$$W' = \tilde{D}_1 W + H(z_1, z_2, \bar{z}_2, W; \mu). \tag{20}$$

For the map (20), there exists a local center manifold $W(z_1, z_2, \bar{z}_2; \mu)$ [50,51], which can be determined by the following equation:

$$W(z_1', z_2', \bar{z}_2'; \mu) = \tilde{D}_1 W(z_1, z_2, \bar{z}_2; \mu) + H(z_1, z_2, \bar{z}_2, W(z_1, z_2, \bar{z}_2; \mu); \mu). \tag{21}$$

On the center manifold the local behavior of the map (20) can be reduced to a three-dimensional map $\tilde{\Phi}(z; \mu)$, which is now

$$z_1' = \tilde{\lambda}_1(\mu) z_1 + G^{(1)}(z_1, z_2, \bar{z}_2, W(z_1, z_2, \bar{z}_2; \mu); \mu),$$

$$z_2' = \tilde{\lambda}_2(\mu) z_2 + G^{(2)}(z_1, z_2, \bar{z}_2, W(z_1, z_2, \bar{z}_2; \mu); \mu). \tag{22}$$

where the Taylor series expansion of $W(z_1, z_2, \bar{z}_2; \mu)$ and $G_i(z_1, z_2, \bar{z}_2, W(z_1, z_2, \bar{z}_2; \mu); \mu)$ about (0,0,0,μ) can be determined by the method which is introduced in Ref. [51].

By using the center manifold theorem technique and normal form method of maps, we can reduce the map (22) to the normal form map $\Phi(z; \varepsilon)$, which is given by

$$\left.\begin{aligned} z_1' &= z_1 + \varepsilon_1 z_1 + a z_1^2 + b z_2 \bar{z}_2 + g z_1^3 + h z_1 z_2 \bar{z}_2 + O((|z_1| + |z_2|)^5) \\ z_2' &= \tilde{\lambda}_2(0) z_2 + \tilde{\varepsilon}_2 z_2 + \tilde{c} z_1 z_2 + \tilde{e} z_1^2 z_2 + \tilde{m} z_2^2 \bar{z}_2 + O((|z_1| + |z_2|)^5) \end{aligned}\right\}, \tag{23}$$

The normal form map (23), in the real form $\Phi(Y; \varepsilon)$, is expressed by

$$\begin{aligned} y_1' &= y_1 + \varepsilon_1 y_1 + a y_1^2 + b(y_2^2 + y_3^2) + g y_1^3 + h y_1 (y_2^2 + y_3^2) + \text{h.o.t}, \\ y_2' &= (\alpha + \varepsilon_2) y_2 - (\varpi + \varepsilon_3) y_3 + c y_1 y_2 - d y_1 y_3 + e y_1^2 y_2 - f y_1^2 y_3 + m y_2 (y_2^2 + y_3^2) - n y_3 (y_2^2 + y_3^2) + \text{h.o.t}, \\ y_3' &= (\varpi + \varepsilon_3) y_2 + (\alpha + \varepsilon_2) y_3 + c y_1 y_3 + d y_1 y_2 + e y_1^2 y_3 + f y_1^2 y_2 + m y_3 (y_2^2 + y_3^2) + n y_2 (y_2^2 + y_3^2) + \text{h.o.t}. \end{aligned} \tag{24}$$

in which, $\varepsilon = (\varepsilon_1, \varepsilon_2, \varepsilon_3)^{\mathrm{T}}$, $\varepsilon_i = \varepsilon_i(\mu)$, $\varepsilon_i(0) = 0$.

5.2. Local codimension two bifurcation of normal form map

There may exist pitchfork, saddle-node or transcritical bifurcation of period-one double-impact symmetrical motion near the point of codimension two bifurcation. The period-one double-impact symmetrical motion of the system shown in Fig. 1 undergoes pitchfork bifurcation in most cases, so let us assume that there exist the new fixed points of period one for the map $\Phi(Y; \varepsilon)$ near the value of codimension two bifurcation, caused by pitchfork bifurcation. In view of the normal form map (24), the new fixed points of period one, represented by Y^*, satisfy the equation

$$\Phi(Y^*; \varepsilon_1, \varepsilon_2, \varepsilon_3) = Y^*. \tag{25}$$

Ignoring the terms of high order of ε, the solutions of Eq. (25) become

$$Y_0^* = (0,0,0)^{\mathrm{T}}, \quad Y_1^* = \left(\frac{-a + \sqrt{a^2 - 4g\varepsilon_1}}{2g}, 0, 0\right)^{\mathrm{T}}, \quad Y_2^* = \left(\frac{-a - \sqrt{a^2 - 4g\varepsilon_1}}{2g}, 0, 0\right)^{\mathrm{T}}. \tag{26}$$

$Y_0^* = (0,0,0)^{\mathrm{T}}$ is the trivial fixed point of period one. If $a = b = \tilde{c} = 0$ [2] and $\varepsilon_1/g < 0$ then there exist the fixed points of period one Y_{1P}^* and Y_{2P}^* caused by pitchfork bifurcation, which are expressed by

$$Y_{1P}^* = \left(\sqrt{-\frac{\varepsilon_1}{g}}, 0, 0\right)^{\mathrm{T}}, \quad Y_{2P}^* = \left(-\sqrt{-\frac{\varepsilon_1}{g}}, 0, 0\right)^{\mathrm{T}}. \tag{27}$$

They are symmetrical at the origin due to symmetry of the structure and excitation point. The fixed point of period one Y_{1P}^* or Y_{2P}^* may be born by giving different initial conditions of map, respectively.

The linearized maps of $\Phi(Y; \varepsilon)$ at the fixed point Y_0^* and Y_{1P}^* (or Y_{2P}^*), respectively, are given by

$$Q_0 = \left.\frac{\partial \Phi(Y, \varepsilon)}{\partial Y}\right|_{(Y_0^*, \varepsilon)} = \begin{bmatrix} 1 + \varepsilon_1 & 0 & 0 \\ 0 & \alpha + \varepsilon_2 & -(\varpi + \varepsilon_3) \\ 0 & \varpi + \varepsilon_3 & \alpha + \varepsilon_2 \end{bmatrix}, \tag{28}$$

$$Q_P = \left.\frac{\partial \Phi(Y, \varepsilon)}{\partial Y}\right|_{(Y_{iP}^*, \varepsilon)} = \begin{bmatrix} r & 0 & 0 \\ 0 & p & q \\ 0 & -q & p \end{bmatrix} \quad (i = 1, 2), \tag{29}$$

in which, $r = 1 - 2\varepsilon_1$, $p = \alpha - e/g\varepsilon_1 + \varepsilon_2$, $q = -\varpi + f/g\varepsilon_1 - \varepsilon_3$.

The partial bifurcation sets for the normal form map (24) can be determined by computing and analyzing the eigenvalues of Jacobian matrixes (28) and (29), respectively. However, a full understanding of the normal form map (24) requires more than Jacobian matrixes (28) and (29). So it is necessary to change the normal form map (23) to the polar coordinate form $\Phi(r, \theta; \varepsilon_0) \in \mathbf{R}^2 \times \mathbf{S}$, $(x, r, \theta) \to (x', r', \theta')$.

Let $\tilde{\varepsilon}_2 = \tilde{\lambda}_2(0)\tilde{\varepsilon}_{20}$, $\varepsilon_0 = (\varepsilon_1, \varepsilon_{20})^{\mathrm{T}}$, $\tilde{c} = \tilde{\lambda}_2(0)\tilde{c}_0$, $\tilde{e} = \tilde{\lambda}_2(0)\tilde{e}_0$, $\tilde{m} = \tilde{\lambda}_2(0)\tilde{m}_0$, the normal form map (23) becomes

$$\begin{aligned} z_1' &= z_1 + \varepsilon_1 z_1 + a z_1^2 + b z_2\bar{z}_2 + g z_1^3 + h z_1 z_2\bar{z}_2 + O((|z_1| + |z_2|)^5), \\ z_2' &= \tilde{\lambda}_2(0) z_2(1 + \tilde{\varepsilon}_{20} + \tilde{c}_0 z_1 + \tilde{e}_0 z_1^2 + \tilde{m}_0 z_2\bar{z}_2) + O((|z_1| + |z_2|)^5). \end{aligned} \tag{30}$$

In polar coordinates, the map $\Phi(z; \varepsilon_0) \in \mathbf{R}^3$ is changed to $\Phi(x, r, \theta; \varepsilon_0) \in \mathbf{R}^2 \times \mathbf{S}$, which is given by

$$\begin{aligned} x' &= x + \varepsilon_1 x + a x^2 + b r^2 + g x^3 + h x r^2 + \text{h.o.t}, \\ r' &= r(1 + \varepsilon_{20} + c_0 x + e_0 x^2 + m_0 r^2) + \text{h.o.t}, \\ \theta' &= \theta + \theta_0 + \varepsilon_{30} + d_0 x + f_0 x^2 + n_0 r^2 + \text{h.o.t} \end{aligned} \tag{31}$$

in which, $\varepsilon_{20} = \alpha\varepsilon_2 + \varpi\varepsilon_3$, $\varepsilon_{30} = \alpha\varepsilon_3 - \varpi\varepsilon_2$, $e_0 = \alpha e + \varpi f$, $f_0 = \alpha f - \varpi e$, $m_0 = \alpha m + \varpi n$, $n_0 = \alpha n - \varpi m$.

We ignore the influence of phase angle θ to the map (31) temporarily. By the map, a two-dimensional map is obtained, which is now

$$\begin{aligned} x' &= x + \varepsilon_1 x + a x^2 + b r^2 + g x^3 + h x r^2 + \text{h.o.t}, \\ r' &= r(1 + \varepsilon_{20} + c_0 x + e_0 x^2 + m_0 r^2) + \text{h.o.t}, \end{aligned} \tag{32}$$

if $a = b = \tilde{c}_0 = 0$, the map (32) becomes

$$x' = x(1 + \varepsilon_1 + g x^2 + h r^2) + \text{h.o.t}, \quad r' = r(1 + \varepsilon_{20} + e_0 x^2 + m_0 r^2) + \text{h.o.t}, \tag{33}$$

for which there exist the fixed points of period one caused by pitchfork bifurcation.

The map (33) has four fixed points:

$$Y_0 = (0,0)^{\mathrm{T}}, \quad Y_{0T} = \left(0, \sqrt{\frac{-\varepsilon_{20}}{m_0}}\right)^{\mathrm{T}}, \quad Y_{1P} = \left(\sqrt{\frac{-\varepsilon_1}{g}}, 0\right)^{\mathrm{T}}, \quad \left(\text{or } Y_{2P} = \left(-\sqrt{\frac{-\varepsilon_1}{g}}, 0\right)^{\mathrm{T}}\right),$$

$$Y_{1T} = \left(\sqrt{\frac{m_0\varepsilon_1 - h\varepsilon_{20}}{e_0 h - m_0 g}}, \sqrt{\frac{g\varepsilon_{20} - e_0\varepsilon_1}{e_0 h - m_0 g}}\right)^{\mathrm{T}} \quad \left(\text{or } Y_{2T} = \left(-\sqrt{\frac{m_0\varepsilon_1 - h\varepsilon_{20}}{e_0 h - m_0 g}}, \sqrt{\frac{g\varepsilon_{20} - e_0\varepsilon_1}{e_0 h - m_0 g}}\right)^{\mathrm{T}}\right).$$

Two simple cases and a complex case are considered. We first analyze the unfolding of the simple case (I) associated with a scheme of coefficients of high order terms: $g<0$, $m_0<0$, $h<0$, $e_0<0$, $g<e_0$, $h<m_0$ and $e_0 h - m_0 g<0$. Stable conditions of these fixed points can be determined by computing and analyzing of eigenvalues of corresponding Jacobian matrix, respectively.

$Y_0 = (0,0)^{\mathrm{T}}$ is the trivial fixed point of map (33), local stable condition of which is $\varepsilon_1<0$ and $\varepsilon_{20}<0$. It should be noted that the existence of the fixed point $Y_1 = (0, \sqrt{-\varepsilon_{20}/m_0})^{\mathrm{T}}$ requires the condition $\varepsilon_{20}/m_0<0$, local stable condition of the fixed point Y_1 is $\varepsilon_1<h\varepsilon_{20}/m_0$ and $\varepsilon_{20}>0$. The existence of the fixed point Y_{1P} (or Y_{2P}) requires the condition $\varepsilon_1/g<0$, and local stable condition of the fixed point is $\varepsilon_1>0$, $\varepsilon_{20}<e_0\varepsilon_1/g$. The existence of the fixed point Y_{1T} (or Y_{2T}) requires the condition $(m_0\varepsilon_1 - h\varepsilon_{20})/(e_0 h - m_0 g)>0$ and $(g\varepsilon_{20} - e_0\varepsilon_1)/(e_0 h - m_0 g)>0$ (according to $e_0 h - m_0 g<0$, the existent region of the fixed point Y_{1T} (or Y_{2T}) can be given by $\varepsilon_{20}>e_0\varepsilon_1/g$ and $\varepsilon_{20}<m_0\varepsilon_1/h(\varepsilon_1>0)$), and local stable conditions of the fixed point Y_{1T} (or Y_{2T}) are $\varepsilon_1>0$, $\varepsilon_{20}>e_0\varepsilon_1/g$ and $\varepsilon_{20}<m_0(g-e_0)\varepsilon_1/(gh - gm_0)$.

Local behavior of the map (33) is not only determined by ε_1 and ε_{20}, but also by the coefficients of high order terms of the map. We consider the influence of phase angle θ to the map (33) to analyze the unfolding of the map (24). By making a comparison between the simplified map (33) and normal form map (24), we can unfold qualitative analyses for the normal form map. The fixed point Y_0 of the map (33) corresponds to the trivial fixed point $Y_0^* = (0,0,0)^{\mathrm{T}}$ of the normal form map (24). The fixed point Y_{0T} of the map (33) corresponds to the invariant circle of the normal form map (24) which is associated with the fixed point Y_0^*; the fixed point Y_{1P} (or Y_{2P}) of the map (33) corresponds to the fixed point Y_{1P}^* (or Y_{2P}^*) of the normal form map (24), caused by pitchfork bifurcation; the fixed point Y_{iT} of the map (33) corresponds to the invariant circle of the map (24), associated with the fixed point Y_{iP}^*. For the map (24), the trivial fixed point Y_0^* loses its stability upon crossing the half-line L_1: $\varepsilon_1 = 0$, $\varepsilon_{20}<0$, and the other fixed point Y_{1P}^* (or Y_{2P}^*) bifurcates simultaneously from the trivial fixed point Y_0^* via a pitchfork bifurcation. On the line L_4: $\varepsilon_{20} = m_0\varepsilon_1/h(\varepsilon_1>0)$, Hopf bifurcation associated with the fixed point Y_{iP}^* occurs for the map (24), and a closed circle associated

with the fixed point Y^*_{1P} (or Y^*_{2P}) exists in region R_4. On the line L_5: $\varepsilon_{20} = m_0(g-e_0)\varepsilon_1/(gh-gm_0)(\varepsilon_1>0)$, the invariant circle associated with the fixed point Y^*_{iP} will change its stability, and torus bifurcation occurs, which possibly results in torus doubling, phase locking or quasi-attracting invariant circle, etc. The trivial fixed point Y^*_0 loses its stability upon crossing the half-line L_2: $\varepsilon_{20} = 0\,(\varepsilon_1<0)$, and a closed circle bifurcates from the trivial fixed point Y^*_0 via a non-degenerate Hopf bifurcation. On the line L_3: $\varepsilon_{20} = m_0\varepsilon_1/h\,(\varepsilon_1>0)$, the invariant circle associated with the fixed points Y^*_0 will change its stability, and torus bifurcation occurs, which possibly leads to torus doubling, phase locking or quasi-attracting invariant circle, etc.

In the present case of scheme of coefficients of high order terms: $g<0$, $m_0<0$, $h<0$, $e_0<0$, $e_0h-m_0g<0$, $h-m_0<0$, the bifurcation set for map (33), near the critical point $\varepsilon = (\varepsilon_1, \varepsilon_{20})^{\mathrm{T}} = (0,0)^{\mathrm{T}}$, can be illustrated by Fig. 2. Only the positive (x, r) quadrant is shown in Fig. 2. The fixed points Y_{2P} and Y_{2T} in the $(-x, r)$ quadrant are not plotted in Fig. 2. Since the portraits are symmetric under reflection about r axis. The bounds of the regions shown in Fig. 2 can be listed as follows:

$$
\begin{aligned}
&L_1 = \{(\varepsilon_1,\ \varepsilon_{20}) : \varepsilon_1 = 0, \varepsilon_{20}<0\}, \quad L_2 = \{(\varepsilon_1,\ \varepsilon_2) : \varepsilon_{20} = 0, \varepsilon_1<0\},\\
&L_3 = \left\{(\varepsilon_1,\ \varepsilon_{20}) : \varepsilon_{20} = \frac{m_0}{h}\varepsilon_1, \varepsilon_1>0\right\}, \quad L_4 = \left\{(\varepsilon_1,\ \varepsilon_2) : \varepsilon_{20} = \frac{e_0}{g}\varepsilon_1, \varepsilon_1>0\right\},\\
&L_5 = \left\{(\varepsilon_1,\ \varepsilon_{20}) : \varepsilon_{20} = \frac{m_0(g-e_0)}{g(h-m_0)}\varepsilon_1,\ \ \varepsilon_1>0\right\}.
\end{aligned}
\tag{34}
$$

We analyze the unfolding of the case (II) associated with a scheme of coefficients of high order terms: $g<0$, $m_0>0$, $h<0$, $e_0>0$ and $e_0h-m_0g<0$. The formulae of the bounds L_1–L_5 of the regions, shown in Fig. 3, are the same algebraically as those in simple case (I).

Let us analyze the local behavior of the normal form map (24) near the bifurcation point $\varepsilon = (0,0,0)^{\mathrm{T}}$ by means of Fig. 3. By comparison with Fig. 2, we can find that pitchfork bifurcation and further transition of the normal form map in the case (II) are similar to those in the case (I). However, the difference is that Hopf bifurcation of normal form map associated with the fixed point $Y^{(1)}_0$ in the case (I) is supercritical; in the case (II), subcritical. The difference of the unfolding of two cases can be observed obviously in the third and fourth quadrants of Figs. 2 and 3. In the sector region R_3, there exist fixed points Y_0, Y_{0T}, Y_{iP} and Y_{iT}. However, only the fixed point Y_{1T} (or Y_{2T}) is stable, and others unstable. By analyzing the Jacobian matrix of map (33), we can obtain two real eigenvalues associated with the fixed points Y_{iT} in the sector region R_3, one of which escapes the unit circle from the point (1,0) upon crossing the half-line L_5. The fixed point Y_{1T} (or Y_{2T}) is stable node in the region R_3, and not unstable in the sector region R_4. It is to be noted that very complicated behavior

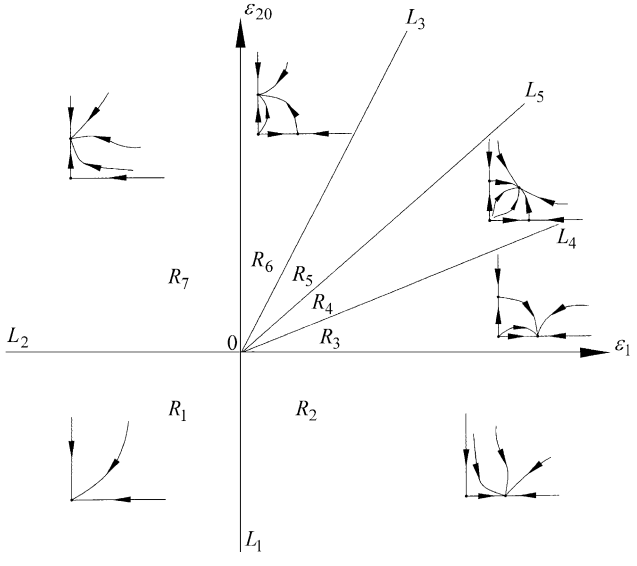

Fig. 2. Unfolding of case (I), $g<0$, $m_0<0$, $h<0$, $e_0<0$, $g<e_0$, $h<m_0$ and $e_0h-m_0g<0$. Bifurcation set of map (33).

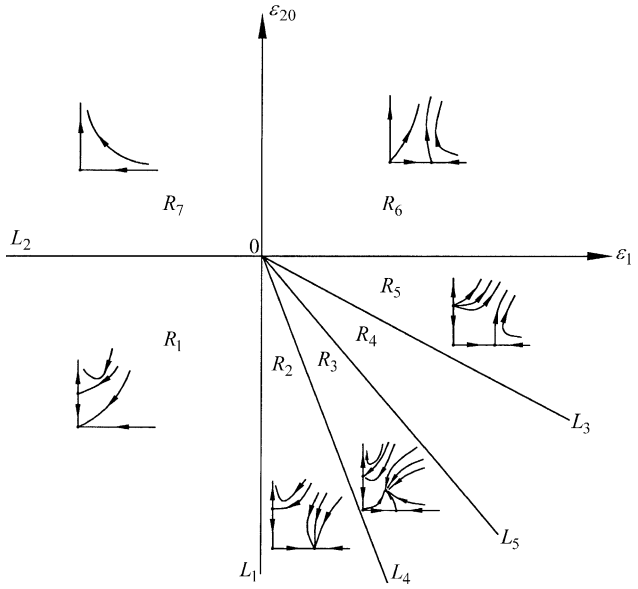

Fig. 3. Unfolding of case (II), $g<0$, $m_0>0$, $h<0$, $e_0>0$ and $e_0h-m_0g<0$. Bifurcation set of map (33).

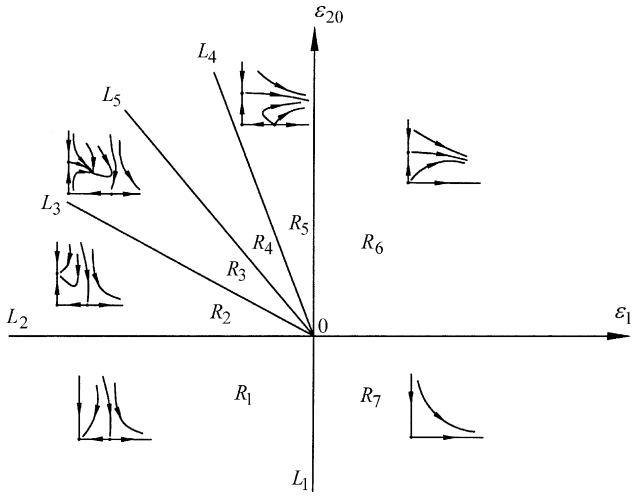

Fig. 4. Unfolding of a complex case (III), $g>0$, $m_0<0$, $h>0$, $e_0<0$ and $e_0h-m_0g<0$. Bifurcation set of map (33).

occur in region R_4, i.e., there exists possibly tori doubling, phasing locking or quasi-attracting invariant circle for the normal form in the region.

Now we continue to analyze the unfolding of the complex case (III) associated with a scheme of coefficients of high order terms: $g>0$, $m_0<0$, $h>0$, $e_0<0$ and $e_0h-m_0g<0$. The bifurcation set of map (33) in the case (III) is shown in Fig. 4. The bounds of the regions shown in Fig. 4 can be listed as follows:

$$L_1=\{(\varepsilon_1,\ \varepsilon_{20}):\varepsilon_1=0,\varepsilon_{20}<0\},\quad L_2=\{(\varepsilon_1,\ \varepsilon_2):\varepsilon_{20}=0,\varepsilon_1<0\},$$

$$L_3=\left\{(\varepsilon_1,\ \varepsilon_{20}):\varepsilon_{20}=\frac{m_0}{h}\varepsilon_1,\varepsilon_1<0\right\},\quad L_4=\left\{(\varepsilon_1,\ \varepsilon_2):\varepsilon_{20}=\frac{e_0}{g}\varepsilon_1,\varepsilon_1<0\right\},$$

$$L_5=\left\{(\varepsilon_1,\ \varepsilon_{20}):\varepsilon_{20}=\frac{m_0(g-e_0)}{g(h-m_0)}\varepsilon_1,\ \ \varepsilon_1<0\right\}.$$

By making a comparison between the map (33) and normal form map (24), we can unfold qualitative analyses for the normal form map in the case (III). Now we analyze the local behavior of the normal form map (24) near the bifurcation point $\varepsilon = (0,0,0)^{\mathrm{T}}$ by means of Fig. 4. For the normal form map (24), in region R_1 we have two fixed points, the stable trivial fixed point $Y_0^{(1)} = (0,0,0)^{\mathrm{T}}$ and unstable fixed point Y_{1P}^* (or Y_{2P}^*). As we have known, the trivial fixed point is node/focus, and the fixed point Y_{1P}^* (or Y_{2P}^*) is saddle in the region R_1. As the parameters cross the line L_2 from the region R_1, Hopf bifurcation of the trivial fixed point $Y_0^{(1)}$ occurs so that a quasi-periodic attractor represented by the attracting closed circle is generated in region R_2, and the fixed point Y_{1P}^* (or Y_{2P}^*) retains its sense. As the parameters cross the line L_3 from the region R_2, the closed circle becomes non-attracting and the torus bifurcation occurs, which causes that a new closed circle is born. The closed circle is attracting in region R_3, and non-attracting in region R_4. In region R_5, there exist the unstable trivial fixed point, unstable fixed point Y_{1P}^* (or Y_{2P}^*) and non-attracting invariant circle associated with the trivial fixed point. In region R_6, we have the unstable trivial fixed point and non-attracting invariant circle associated with the trivial fixed point.

It is to be noted that the closed circles of the normal form map (24), in region R_4 of Fig. 2, regions R_3 of Figs. 2 and 3, are born by different ways. In cases (I) and (II), the closed circle is generated via Hopf bifurcation of the fixed point Y_{1P}^* (or Y_{2P}^*); in case (III) by torus bifurcation.

The bifurcation sets for the map (24), corresponding to the other cases of scheme of coefficients of high order terms, can be obtained by the similar method used in three cases above-mentioned.

In view of the Jacobian matrixes (28) and (29), we can find that there exist the period one point Y_{1P}^* (or Y_{2P}^*) for $\varepsilon_1/g<0$. According to the unfolding of the simple case (I), the bifurcation set of the map (24), near $\varepsilon = (0,0,0)^{\mathrm{T}}$, can be further illustrated by Fig. 5. Three possible cases for $\lambda_1, \lambda_{2,3}$ of Jacobian matrix Q_0 escaping the unit circle are shown in Fig. 6. The unfolding of normal form map (24), corresponding to the cases (II) and (III), can be obtained by the similar method used in the present case. The bounds of the regions shown in Fig. 5 can be listed as follows:

$$\begin{aligned}
&\alpha g\varepsilon_2 + \varpi g\varepsilon_3 - (\alpha e + \varpi f)\varepsilon_1 = 0,\\
&L_{11}: \varepsilon_1 = 0, \varepsilon_2 < 0, \quad L_{12}: \varepsilon_2 = 0, \varepsilon_1 < 0, \quad L_{13}: \varepsilon_2 = \frac{\alpha e + \varpi f}{\alpha g}\varepsilon_1, \varepsilon_1 > 0,\\
&L_{21}: \varepsilon_1 = 0, \varepsilon_3 < 0, \quad L_{22}: \varepsilon_3 = 0, \varepsilon_1 < 0, \quad L_{23}: \varepsilon_3 = \frac{\alpha e + \varpi f}{\varpi g}\varepsilon_1, \varepsilon_1 > 0.
\end{aligned} \tag{35}$$

$$\begin{aligned}
&\alpha\varepsilon_2 + \varpi\varepsilon_3 - \frac{(\alpha m + \varpi n)(g - \alpha e - \varpi f)}{g(h - \alpha m - \varpi n)}\varepsilon_1 = 0,\\
&L_{14}: \varepsilon_2 = \frac{(\alpha m + \varpi n)(g - \alpha e - \varpi f)}{\alpha g(h - \alpha m - \varpi n)}\varepsilon_1, \varepsilon_1 > 0, \quad L_{24}: \varepsilon_2 = \frac{(\alpha m + \varpi n)(g - \alpha e - \varpi f)}{\varpi g(h - \alpha m - \varpi n)}\varepsilon_1, \varepsilon_1 > 0.
\end{aligned} \tag{36}$$

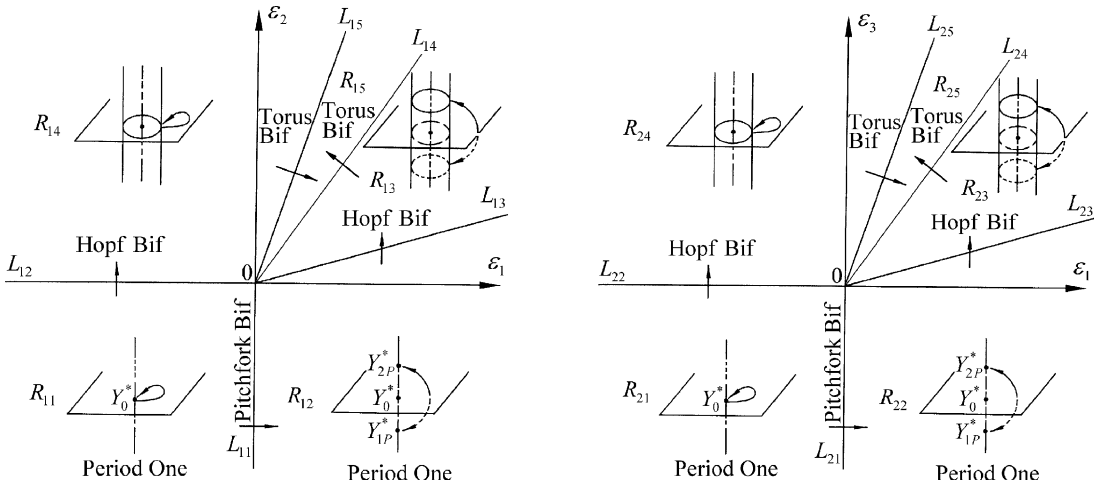

Fig. 5. Bifurcation set of the normal form map (24) in the case (I).

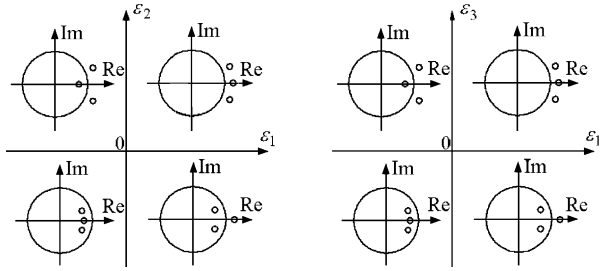

Fig. 6. Three possible cases for $\lambda_1, \lambda_{2,3}$ of Jacobian matrix Q_0 escaping the unit circle, in case (I).

$$\alpha h\varepsilon_2 + \varpi h\varepsilon_3 - (\alpha m + \varpi n)\varepsilon_1 = 0,$$
$$L_{15} : \varepsilon_2 = \frac{\alpha m + \varpi n}{\alpha h}\varepsilon_1, \varepsilon_1 > 0, \quad L_{25} : \varepsilon_2 = \frac{\alpha m + \varpi n}{\varpi h}\varepsilon_1, \varepsilon_1 > 0. \tag{37}$$

Here we can assume, without loss of generality, $\alpha > 0$. In formulae (35)–(37), $\alpha e + \varpi f = e_0 < 0$, $\alpha m + \varpi n = m_0 < 0$, $g - \alpha e - \varpi f = g - e_0 < 0$ and $h - \alpha m - \varpi n = h - m_0 < 0$.

By analyzing the eigenvalues of Jacobian matrix Q_0 and Q_P, we can conclude that when the parameters pass across the regions as $R_{i1} \to R_{i2}$ $(i = 1,2)$, the type of the fixed point of period one changes from Y_0^* to Y_{1P}^* (or Y_{2P}^*); see Figs. 2 and 5. When the parameters cross the line L_{i1}, the pitchfork bifurcation associated with the fixed point Y_0^* occurs. When the parameters pass across the regions as $R_{i2} \to R_{i3}$, then the type of period one point Y_{1P}^* (or Y_{2P}^*) changes as stable node → stable focus → unstable focus. On the line L_{i3}, Hopf bifurcation associated with the fixed point Y_{1P}^* (or Y_{2P}^*) takes place. When the parameters pass across the regions as $R_{i1} \to R_{i4}$, the type of the fixed point of period one Y_0^* changes from stable focus to unstable focus, and on the line L_{i2}, Hopf bifurcation associated with the fixed point Y_0^* occurs. The direction of Hopf bifurcation (supercritical or subcritical) depends on the coefficients of high order terms of the normal form map.

By analysis of unfolding of the map (24) in the present case, we can find that on the line L_{i4} the invariant circle associated with the fixed point Y_{iP}^* changes its stability, and torus bifurcation occurs. On the line L_{i5} the invariant circle associated with the fixed point Y_0^* changes its stability, and torus bifurcation occurs.

According to the center manifold theory, local behavior of the map $\tilde{f}(v, X)$, near the bifurcation point v_c, is equivalent to that of $\Phi(Y; \varepsilon)$ for ε near $\varepsilon = (0, 0, 0)^{\mathrm{T}}$. By virtue of the analysis of local bifurcation of the normal form map (24), we can find out dynamical behavior of the vibro-impact system in the case of codimension two bifurcation considered. Local behavior of the map $\tilde{f}(v, X)$, near the bifurcation point v_c, conforms to the numerical results below.

6. Numerical analysis

The local stability analysis, discussed in the previous section, can reveal different kinds of bifurcations of 1–1–1 symmetrical motions namely Hopf, saddle-node, pitchfork and codimension two bifurcation, etc. In this section the analysis developed in the former section is verified by the presentation of results for a two-degree-of-freedom vibratory system shown in Fig. 7. The existence and stability of period-one double-impact symmetrical motion are analyzed explicitly. Also, local bifurcations at the points of change in stability, discussed in the previous section, are considered, thus giving some information on dynamical behavior near the point of codimension two bifurcation.

The two-degree-of-freedom vibratory system, with system parameters (1): $m_1 = 1.0$, $m_2 = 5.6$, $k_1 = 1.0$, $k_2 = 6.2$, $f_{10} = 1.0$, $f_{20} = 0.0$, $\zeta_1 = 0.001$, $\zeta_2 = 0.0062$ and $R = 0.82$, has been chosen for analyzing the question. The forcing frequency ω and clearance δ are taken as the control parameters, i.e. $v = (\delta, \omega)^{\mathrm{T}}$. The eigenvalues of $\mathrm{D}f(v, 0)$ are computed with $\omega \in [6.0, 8.7]$ and $\delta \in [0.015, 0.04]$. All eigenvalues of $\mathrm{D}f(v, 0)$ stay inside the unit circle for $v = (0.04, 6.0)^{\mathrm{T}}$. By increasing the forcing frequency ω and decreasing the value of clearance δ gradually from the point $v = (0.04, 6.0)^{\mathrm{T}}$ to change the control parameter v, we found that there exist a real eigenvalue $\lambda_1(v_c) = 1.0000002$ and a complex conjugate pair of eigenvalues

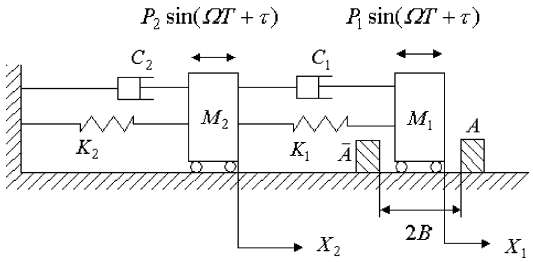

Fig. 7. Schematic of a two-degree-of-freedom vibratory system with symmetrical rigid stops.

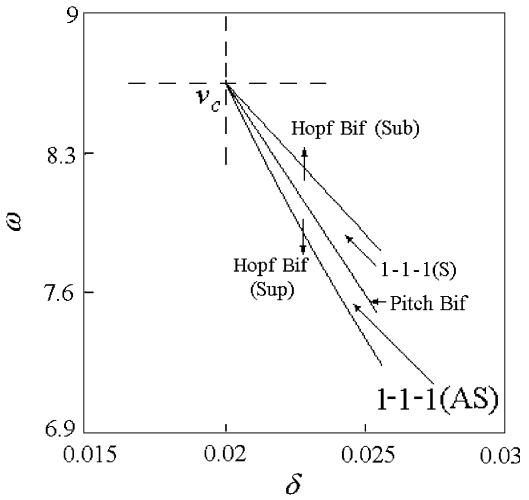

Fig. 8. Partial bifurcation set near the point of codimension two bifurcation.

$\lambda_{2,3}(v_c) = 0.66776710 \pm 0.74313420\mathrm{i}$ ($|\lambda_{2,3}(v_c)| = 0.9991$), which are very close to the unit circle, and the eigenvalue $\lambda_4(v)$ still stays inside the unit circle ($\lambda_4(v_c) = 0.45218780$) as v equals $v_c = (0.019998, 8.492056)^{\mathrm{T}}$. The eigenvalues $\lambda_1(v)$ and $\lambda_{2,3}(v)$ have already escaped the unit circle as ω (increasingly) and δ (decreasingly) pass through $\omega = 8.492057$ and $\delta = 0.019996$. The eigenvalues $\lambda_1(v)$ and $\lambda_{2,3}(v)$ almost escape the unit circle simultaneously, and $v_c = (0.019998, 8.492056)^{\mathrm{T}}$ may be approximately taken as the value of codimension two bifurcation, involving a positive real eingevalue and a complex conjugate pair escaping the unit circle simultaneously.

Numerical analyses are carried out to unfold dynamic behavior of the two-degree-of-freedom vibro-impact system near the point of codimension two bifurcation. The partial bifurcation set, near the value of bifurcation, is plotted in Fig. 8, in which 1–1–1 symmetrical motion is represented by (S), and 1–1–1 antisymmetrical one by (AS). The whole dynamical transitions from simulation are shown in the bifurcation diagrams for the clearance value $\delta = 0.025$ (Fig. 9) in which the velocities of mass M_1, immediately after impact, are shown versus the varying forcing frequency ω. One can observe, from Figs. 8 and 9, that there exists the window of period-one double-impact symmetrical motion in the bifurcation diagrams. The width of the window of 1–1–1 symmetrical motion increases with increase in the value of clearance δ, and the width of the window shrinks to zero at the critical value $v = v_c$. The 1–1–1 symmetrical motion will undergo pitchfork bifurcation with decrease in the forcing frequency ω so that a pair of antisymmetrical double-impact periodic orbits are born. With further decrease in the forcing frequency ω, the 1–1–1 antisymmetrical motions will lose stability, these motions then each undergo supercritical Hopf bifurcation so that the system exhibits quasi-periodic impact motion associated with 1–1–1 antisymmetrical motion, which eventually results in apparently nonperiodic, or chaotic motions via torus doubling, phase locking or quasi-attracting invariant torus. Moreover, the 1–1–1 symmetrical motion undergoes also subcritical Hopf bifurcation with increase in ω. Some projected Poincaré sections are plotted for $\delta = 0.025$ in Figs. 10–12. The Poincaré section is taken

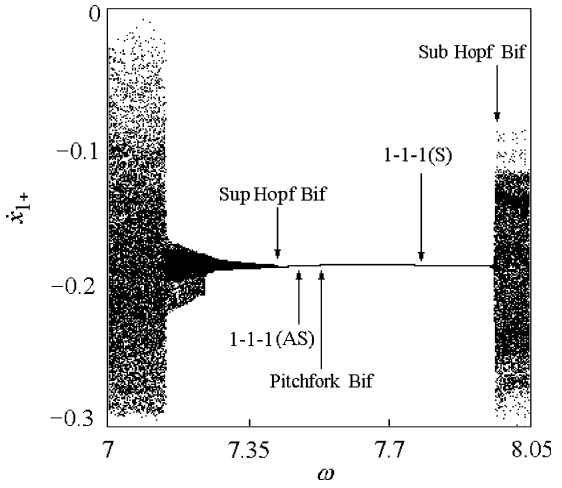

Fig. 9. Bifurcation diagram near the point of codimension two bifurcation, $\delta = 0.025$.

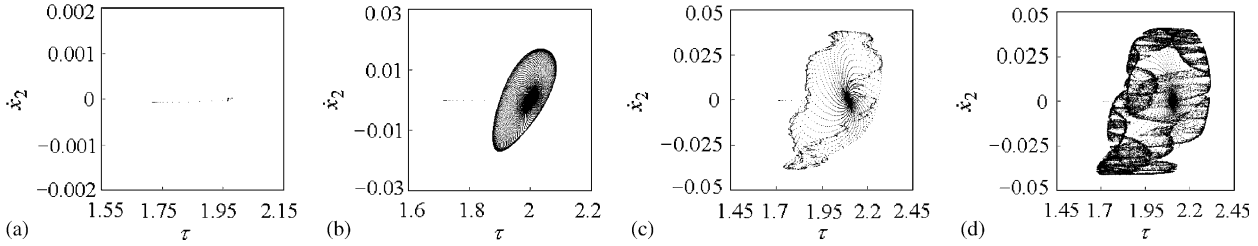

Fig. 10. The projected Poincaré sections: (a) transient points as well as the fixed point associated with 1–1–1 antisymmetrical motion, starting from the initial condition near the fixed point of 1–1–1 symmetrical motion, $\omega = 7.45$; (b) transient points as well as the attracting invariant circle associated with 1–1–1 antisymmetrical point, starting from the initial condition near the fixed point of 1–1–1 symmetrical motion, $\omega = 7.41$; (c) attracting invariant circle of 1–1–1 antisymmetrical point, $\omega = 7.27$; (d) chaos, $\omega = 7.266$.

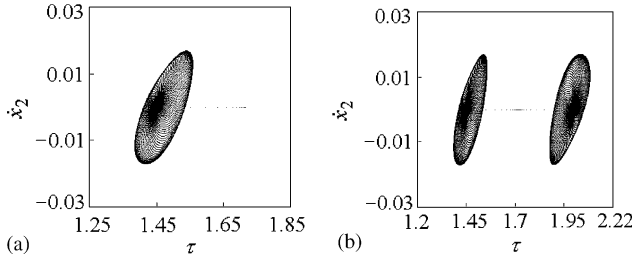

Fig. 11. Projected Poincaré sections: (a) attracting invariant circle of 1–1–1 antisymmetrical point, $\omega = 7.41$; (b) a comparison of symmetry of two quasi-periodic attractors about the original fixed point $\omega = 7.41$.

in the form $\sigma = \{(x_1, \dot{x}_1, x_2, \dot{x}_2, \theta) \in \mathbf{R}^4 \times \mathbf{S},\ x_1 = \delta,\ \dot{x}_1 = \dot{x}_{1+}\}$, which is four-dimensional. The section is projected to the $(\tau, \dot{x}_2)$ or $(\tau, \dot{x}_{1+})$ plane, etc., which is called the projected Poincaré section. The fixed point associated with 1–1–1 symmetrical motion, with the corresponding parameter v, is taken as the initial map point in every numerical analysis. We choose the value of clearance $\delta = 0.025$ and change the forcing frequency ω in the following analyses. It is shown, by numerical results, that the system exhibits stable 1–1–1 symmetrical motion with $\omega \in (7.590414, 7.883305)$; see Fig. 9.

The 1–1–1 symmetrical motion has changed its stability, and pitchfork bifurcation associated with the motion occurs as ω is decreased gradually and passes through $\omega_{c1} = 7.590414$, i.e., the system exhibits stable

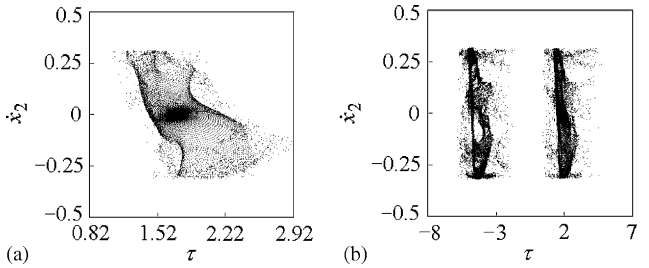

Fig. 12. Projected Poincaré sections: (a) local map near the unstable fixed point of 1–1–1 symmetrical motion, $\omega = 8.0$ (3000 impacts); (b) transient points as well as chaotic attractor, starting from the initial condition near the fixed point of 1–1–1 symmetrical motion, $\omega = 8.0$ (15 000 impacts).

1–1–1 antisymmetrical motion as seen in Figs. 9 and 10(a). Transient points as well as the fixed point associated with 1–1–1 antisymmetrical motion, starting from the initial condition near the unstable fixed point of 1–1–1 symmetrical motion, are ploted for $\omega = 7.45$ in Fig. 10(a). Two different orbits with antisymmetrical double-impact characteristic are possibly caused by different initial conditions, respectively. With further decrease in the forcing frequency ω, the 1–1–1 antisymmetrical motions will change stability, these motions then each undergo Hopf bifurcations. The system, shown in Fig. 7, exhibits quasi-periodic motion associated with 1–1–1 antisymmetrical one. The quasi-periodic attractor is represented by an attracting invariant circle in projected Poincaré sections; see Figs. 10(b) and (c) which show transient points as well as the attracting invariant circle associated 1–1–1 antisymmetrical point, starting from the initial condition near the unstable fixed point of 1–1–1 symmetrical motion. It is to be noted that the attracting invariant circle is smooth in nature near the value of Hopf bifurcation of 1–1–1 antisymmetrical motion. As the value of ω moves further away from the value of Hopf bifurcation, the attracting invariant circle expands, and the smoothness of quasi-periodic attractor is changed by degrees until it is destroyed. The quasi-periodic impact motion finally transits to chaos via the quasi-attracting invariant circle as ω is changed decreasingly; see Fig. 10(d). The quasi-attracting invariant circle is attracting for the map point inside the circle, and repelling for the map point on or outside it.

A phenomenon needs mentioning. Pitchfork bifurcation of 1–1–1 symmetrical motion may leads to two different orbits with antisymmetrical double-impact characteristic due to different initial conditions, respectively. Hopf bifurcation associated with 1–1–1 antisymmetrical motion may lead to two different quasi-periodic orbits with antisymmetrical characteristic due to different initial conditions, respectively; which is illustrated by Figs. 10(b) and 11(a). A comparison of symmetry of two quasi-periodic attractors about the trivial fixed point can be observed in Fig. 11(b). However, the symmetry of two quasi-periodic attractors, about the trivial fixed point, will be changed as the forcing frequency is further far away the value of Hopf bifurcation.

The 1–1–1 symmetrical motion undergoes subcritical Hopf bifurcation as ω passes through $\omega_{c2} = 7.883305$ in a increasing way, which is illustrated by the center manifold theorem technique and normal form method of maps used in Ref. [22]. At the critical value $\omega_{c2} = 7.883305$, the eigenvalues of $Df(\omega, 0)$ and associated bifurcation parameters are given as follows:

$$\lambda_1(\omega_{c2}) = 0.9886617, \quad \lambda_{2,3}(\omega_{c2}) = 0.6193914 \pm 0.7850825\mathrm{i},$$
$$\left|\lambda_{2,3}(\omega_{c2})\right| = 1.0000001, \quad \lambda_4(\omega_{c2}) = 0.4785741,$$
$$\mathrm{d}\lambda_2(\mu)/\mathrm{d}\mu\big|_{\mu=0} = 2.355861, \quad \mu = \omega - \omega_{c2}, \quad f_1(0) = -1.562334.$$

We can conclude, according to the results above-mentioned and Ref. [52], that a subcritical Hopf bifurcation of 1–1–1 symmetrical motion occurs for $\omega > 7.883305$, and a change from stable focus to unstable focus, associated with the fixed point of 1–1–1 symmetrical motion, is generated. The analysis is verified by numerical results. Fig. 12(a) shows local map near the unstable fixed point associated with 1–1–1 symmetrical motion (unstable focus) for $\omega = 8.0$. Fig. 12(b) shows transient points as well as chaotic attractor, starting from the

initial condition near the fixed point associated with 1-1-1 symmetrical motion (unstable focus) for $\omega = 8.0$. The example analyzed corresponds to the unfolding case (II) in Section 5.2.

The system shown in Fig. 7, with parameters (2): $m_1 = 1$, $m_2 = 1.8$, $k_1 = 1$, $k_2 = 4.0$, $f_{10} = 1$, $f_{20} = 0$, $\zeta_1 = 0.0003$ and $\zeta_2 = 0.0012$ has been chosen for analyzing its dynamical behavior near the point of codimension two bifurcation. The forcing frequency ω and the clearance δ are taken as the control parameters, i.e. $v = (\delta, \omega)^{\mathrm{T}}$. The eigenvalues of Jacobian matrix $\mathrm{D}f(v, 0)$ are computed with $\omega \in [3.3, 4.0]$ and $\delta \in [0.08, 0.12]$. All eigenvalues of $\mathrm{D}f(v, 0)$ stay inside the unit circle for $v = (0.1, 3.8)^{\mathrm{T}}$. By gradually increasing ω and decreasing δ from the point $v = (0.1, 3.8)^{\mathrm{T}}$ to change the control parameter v, we can obtain a real eigenvalue $\lambda_1(v_c) = 1.0000016$ and a complex conjugate pair of eigenvalues $\lambda_{2,3}(v_c) = 0.6736258 \pm 0.7390723\mathrm{i}$, $(|\lambda_{2,3}(v_c)| = 0.9999998)$ which are very close to the unit circle, and the other eigenvalue $(\lambda_4(v_c) = 0.6574091)$ still stay inside the unit circle as v equals $v_c = (0.0089917, 3.982374)^{\mathrm{T}}$. The eigenvalues $\lambda_1(v)$ and $\lambda_{2,3}(v)$ have escaped the unit circle as ω (increasingly) and δ (decreasingly) pass through $v_c = (0.009, 3.9825)^{\mathrm{T}}$. The eigenvalues $\lambda_1(v)$ and $\lambda_{2,3}(v)$ almost escape the unit circle simultaneously, so $v_c = (0.0089917, 3.982374)^{\mathrm{T}}$ is approximately taken as the value of codimension two bifurcation.

Local behavior of the system, near the point of codimension two bifurcation, is obtained by numerical simulation. The partial bifurcation set near the critical value is plotted in Fig. 13. As the clearance δ is fixed, the 1–1–1 symmetrical motion will undergo pitchfork bifurcation, with decrease in the forcing frequency ω, so that a pair of antisymmetrical double impact periodic orbits stabilize. With further decrease in ω, instability of 1–1–1 antisymmetrical motions occurs, these motions then each undergo supercritical Hopf bifurcation so that the quasi-periodic impact motions associated with 1–1–1 antisymmetrical one stabilize, which eventually result in apparently non-periodic, or chaotic motions via torus doubling, phase locking or quasi-attracting circle. Whereas the 1–1–1 symmetrical motion undergoes also supercritical Hopf bifurcation with increase in the forcing frequency ω. Dynamical behavior of the system, near the point of codimension two bifurcation, is further illustrated by bifurcation diagram and projected Poincaré sections plotted in Figs. 14–16. The fixed point associated with 1–1–1 symmetrical motion, with the corresponding parameter v, is still taken as the initial map point in every numerical analysis. We choose the clearance value $\delta = 0.1$ and change the forcing frequency ω in the following numerical analysis. The stable 1–1–1 symmetrical motion is shown to exist in the forcing frequency range $\omega \in (3.772726, 3.838787)$; see Fig. 14.

Instability of 1–1–1 symmetrical motion occurs, and pitchfork bifurcation associated with the motion is generated as ω is decreased gradually and passes through $\omega_{c1} = 3.772726$. The system begins to exhibit stable 1–1–1 antisymmetrical motion. The type of fixed point of 1–1–1 antisymmetrical motion, from stable node to

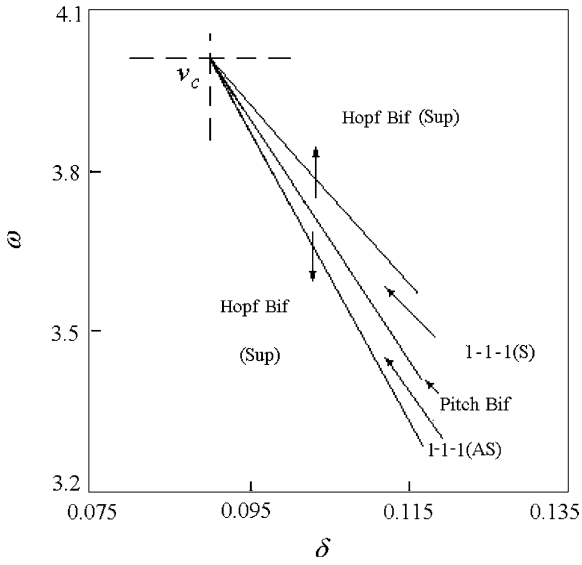

Fig. 13. Partial bifurcation set near the point of codimension two bifurcation.

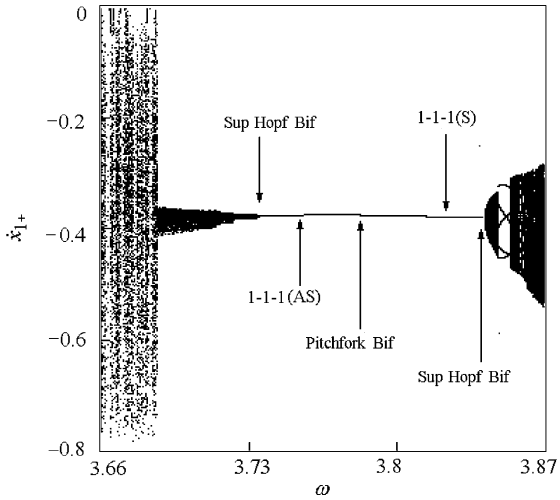

Fig. 14. Bifurcation diagram near the point of codimension two bifurcation, $\delta = 0.1$.

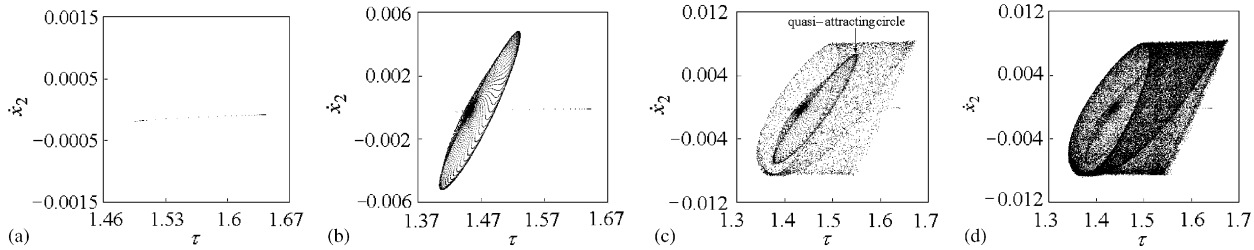

Fig. 15. Projected Poincaré sections: (a) transient points as well as the fixed point associated with 1–1–1 antisymmetrical motion, starting from the initial condition near the fixed point of 1–1–1 symmetrical motion, $\omega = 3.75$; (b) transient points as well as the attracting invariant circle associated with 1–1–1 antisymmetrical point, starting from the initial condition near the fixed point of 1–1–1 symmetrical motion, $\omega = 3.73$; (c) chaos (2500 impacts), $\omega = 3.7225$; (d) chaos (20 000 impacts), $\omega = 3.722$.

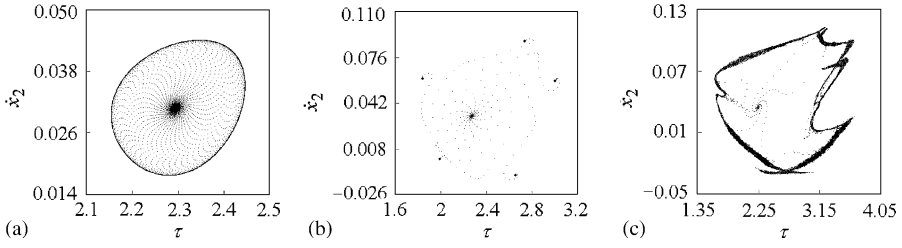

Fig. 16. Projected Poincaré sections: (a) attracting invariant circle associated with the fixed point of 1–1–1 symmetrical motion, $\omega = 3.841$; (b) phase locking, $q = 5/5$ fixed points, $\omega = 3.852$; (c) chaos, $\omega = 3.865$.

stable focus, is changed with decrease in the forcing frequency. With further decrease in ω, instability of 1–1–1 antisymmetrical motions occurs, these motions then undergo Hopf bifurcations. The quasi-periodic attractor is shown in Fig. 15(b). With decrease in ω, the quasi-periodic motion falls into chaotic one. The transition of quasi-periodic attractor to chaos, via the quasi-attracting invariant circle, is illustrated by Figs. 15(c) and (d).

Increase of the forcing frequency leads to instability and supercritical Hopf bifurcation of 1–1–1 symmetrical motion. At the critical value $\omega_{c3} = 3.838787$, the eigenvalues of $Df(\omega, 0)$ and associated

bifurcation parameters are given as follows:

$$\lambda_1(\omega_{c2}) = 0.9882613, \quad \lambda_{2,3}(\omega_{c2}) = 0.7563341 \pm 0.6541861\mathrm{i}, \quad \left|\lambda_{2,3}(\omega_{c2})\right| = 1.000000,$$
$$\lambda_4(\omega_{c2}) = 0.6786712.$$

A supercritical Hopf bifurcation of 1–1–1 symmetrical motion occurs for $\omega > 3.838787$, and a change from stable focus to unstable focus, associated with the fixed point of 1–1–1 symmetrical motion, is generated. Hopf bifurcation of double-impact symmetrical motion and transition to chaos, with increase in the forcing frequency, are shown in Figs. 14 and 16.

By studying codimension two bifurcation of vibro-impact system of Fig. 7, we can find that the system exhibits similar dynamical behavior near the points of codimension two bifurcations. It is to be noted that the second representative example analyzed corresponds to the unfolding case (I) in Section 5.2.

7. Conclusions

A class of multi-degree-of-freedom system having symmetrically placed rigid stops and subjected to periodic excitation is considered. An important application where the model studied here may be of use is in the dynamics of heat exchanger tubes in nuclear reactors [53]. Such tubes are designed to have clearances at support points to allow for thermal expansion. When fluid flows past these tubes vortex shedding occurs and the tubes are excited. The response of such systems is very complicated [53] and the wearing of these tubes is a major problem in the nuclear industry. Fluid flow past panels and beams can result in chaotic motions and thus bifurcation behavior and chaotic motions may provide an appropriate tool in the study of tube wear. Stability and local bifurcations of period-one double-impact symmetrical motion of the vibratory system with symmetrical rigid stops may be analyzed by computing the eigenvalues of Jacobian matrix of linearized Poincaré map. Routes of symmetrical double-impact periodic motions to chaos are also observed by numerical simulation.

Local codimension two bifurcation of maps, involving a real eingevalue and a complex conjugate pair escaping the unit circle simultaneously, is analyzed by using the center manifold technique and normal form method of maps. Dynamical behavior of the vibratory systems with symmetrical rigid stops, near the points of codimension two bifurcations, is investigated by qualitative analyses and numerical simulation. The vibro-impact systems, under the condition of codimension two bifurcations, exhibit more complicated quasi-periodic impact motions than those which occur in the case of codimension one bifurcations. Near the point of codimension two bifurcation there exists not only Hopf and pitchfork bifurcations of 1–1–1 symmetrical motion, but also Hopf bifurcation of 1–1–1 unsymmetrical motion. It is to be noted that no Hopf bifurcation of 1–1–1 symmetrical motion occurs for single degree-of-freedom vibratory system with symmetric stops, see Ref. [2]. However, Hopf bifurcations of 1–1–1 motions are shown to exist in multi-degree-of-freedom vibro-impact system with symmetrical rigid stops.

The strict condition of codimension two bifurcation is not easy to encounter in practical application of engineering. However there exist the possibilities that actual nonlinear dynamical systems, with two varying parameters or more, work near the critical value of codimension two bifurcation due to change of parameters. The impact-forming machinery is a typical example. Besides the forcing frequency ω, the clearance varies also with different thickness of the formed workpieces [54]. Another representative example is the inertial vibro-impact shaker, of which the distribution of masses is generally metabolic with casts of different masses, and the forcing frequency is also important parameter changed [55]. The change of multi-parameters possibly leads to the result that the vibro-impact systems work near the critical parameters of codimension two bifurcation. It is necessary to study the bifurcations caused by change of multi-parameters and reveal dynamical behavior of nonlinear systems near the points of bifurcations.

Acknowledgements

The authors gratefully acknowledge the support by National Natural Science Foundation (10572055, 50475109), Natural Science Foundation of Gansu Province Government of China (ZS-031-A25-007-Z (key item)) and 'Qing Lan' Talent Engineering by Lanzhou Jiaotong University.

Appendix

$$\Phi = \mathrm{diag}[\Psi, \Psi], \quad P_i(t) = \begin{bmatrix} P_{i1}(t) & P_{i2}(t) \\ \dot{P}_{i1}(t) & \dot{P}_{i2}(t) \end{bmatrix}, \quad Q_i(t) = \begin{bmatrix} P_{si}(t) & P_{ci}(t) \\ \dot{P}_{si}(t) & \dot{P}_{ci}(t) \end{bmatrix},$$

$$P_{11}(t) = \mathrm{diag}[g_i(t)\eta_i\omega_i/\omega_{di} + h_i(t)], \quad P_{12}(t) = \mathrm{diag}[g_i(t)/\omega_{di}],$$

$$P_{21}(t) = \mathrm{diag}[\tilde{h}_i(2\pi/\omega)(g_i(t)\eta_i\omega_i/\omega_{di} + h_i(t)) - \tilde{g}_i(2\pi/\omega)(h_i(t)\eta_i\omega_i/\omega_{di} - g_i(t))],$$

$$P_{22}(t) = \mathrm{diag}[(g_i(t)\tilde{h}_i(2\pi/\omega) - \tilde{g}_i(2\pi/\omega)h_i(t))/\omega_{di}],$$

$$P_{si}(t) = \Psi(F_s \cos\,\omega t - F_c \sin\,\omega t + P_{i2}(t)\omega F_c - P_{i1}(t)F_s),$$

$$P_{ci}(t) = \Psi(F_s \sin\,\omega t + P_c \cos\,\omega t - P_{i2}(t)\omega F_s - P_{i1}(t)F_c).$$

where $\tilde{g}_i(t) = \mathrm{e}^{\eta_i\omega_i t}\sin(\omega_{di}t)$, $\tilde{h}_i(t) = \mathrm{e}^{\eta_i\omega_i t}\cos(\omega_{di}t)$, $g_i(t) = \mathrm{e}^{-\eta_i\omega_i t}\sin(\omega_{di}t)$, $h_i(t) = \mathrm{e}^{-\eta_i\omega_i t}\cos(\omega_{di}t)$.

$$\begin{bmatrix} \tilde{A}_1 \\ \tilde{B}_1 \end{bmatrix} = \left[\Phi\tilde{E}(0)\right]^{-1}\begin{bmatrix} x_0 + \Delta x \\ \dot{x}_0 + \Delta\dot{x} \end{bmatrix} - \left[\Phi\tilde{E}(0)\right]^{-1}\Phi U\tilde{Q}\begin{bmatrix} \tilde{S}_{\Delta\tau} \\ \tilde{C}_{\Delta\tau} \end{bmatrix}, \quad \begin{bmatrix} \tilde{A}_2 \\ \tilde{B}_2 \end{bmatrix} = \left[\Phi\tilde{E}(0)\right]^{-1}\begin{bmatrix} \tilde{x}(\tilde{t}_{1+}) \\ \dot{\tilde{x}}(\tilde{t}_{1+}) \end{bmatrix} - \left[\Phi\tilde{E}(0)\right]^{-1}\Phi U\tilde{Q}\begin{bmatrix} \tilde{S}_{\tilde{t}_1} \\ \tilde{C}_{\tilde{t}_1} \end{bmatrix},$$

where $\tilde{S}_{\Delta\tau} = \sin(\tau_0 + \Delta\tau)$, $\tilde{C}_{\Delta\tau} = \cos(\tau_0 + \Delta\tau)$, $\tilde{S}_{\tilde{t}_1} = \sin(\omega\tilde{t}_1 + \tau_0 + \Delta\tau)$, $\tilde{C}_{\tilde{t}_1} = \cos(\omega\tilde{t}_1 + \tau_0 + \Delta\tau)$.

References

[1] P.J. Holmes, *The dynamics of repeated impacts with a sinusoidally vibrating table. Journal of Sound and Vibration* 84 (2) (1982) 173–189.

[2] S.W. Shaw, The dynamics of a harmonically excited system having rigid amplitude constraints. Part 1, Part 2, *Journal of Applied Mechanics* 52 (1985) 453–464.

[3] G.S. Whiston, Global dynamics of vibro-impacting linear oscillator, *Journal of Sound and Vibration* 118 (3) (1987) 395–429.

[4] K.M. Cone, R.I. Zadoks, A numerical study of an impact oscillator with the addition of dry friction, *Journal of Sound and Vibration* 188 (5) (1995) 659–683.

[5] J.O. Aidanpää, B.R. Gupta, Periodic and chaotic behaviour of a threshold-limited two-degree-of-freedom system, *Journal of Sound and Vibration* 165 (2) (1993) 305–327.

[6] F. Peterka, Comments on periodic and chaotic behaviour of a threshold-limited two-degree-of-freedom system, *Journal of Sound and Vibration* 165 (2) (1993) 369–372.

[7] D.Q. Cao, Z.Z. Shu, Periodic motions and robust stability of multi-degree-of-freedom vibrating systems with a clearance, *Acta Mechanica Sinica* 29 (1) (1997) 74–83.

[8] D.J. Wagg, Rising phenomena and the multi-sliding bifurcation in a two-degree-of-freedom impact oscillator, *Chaos, Solitons and Fractals* 22 (3) (2004) 541–548.

[9] Jin Dongping, Hu Haiyan, Periodic vibro-impacts and their stability of a dual component system, *Acta Mechanica Sinica* 13 (4) (1997) 366–376.

[10] Silvio L.T. de Souza, Iberê L. Caldas, Calculation of Lyapunov exponents in systems with impacts, *Chaos, Solitons and Fractals* 19 (3) (2004) 569–579.

[11] A.B. Nordmark, Non-periodic motion caused by grazing incidence in an impact oscillator, *Journal of Sound and Vibration* 145 (2) (1991) 279–297.

[12] G.S. Whiston, Singularities in vibro-impact dynamics, *Journal of Sound and Vibration* 152 (3) (1992) 427–460.

[13] S. Foale, S.R. Bishop, Dynamical complexities of forced impacting systems, *Philosophical Transactions of the Royal Society of London* 338 (A) (1992) 547–556.

[14] A.P. Ivanov, Bifurcation in impact systems, *Chaos, Solitons and Fractals* 7 (10) (1996) 1615–1634.

[15] F. Peterka, Bifurcation and transition phenomena in an impact oscillator, *Chaos, Solitons and Fractals* 7 (10) (1996) 1635–1647.

[16] C. Budd, F. Dux, A. Cliffe, The effect of frequency and clearance variations on single-degree-of-freedom impact oscillators, *Journal of Sound and Vibration* 184 (3) (1995) 475–502.

[17] M.I. Feigin, The increasingly complex structure of the bifurcation tree of a piecewise-smooth system, *Journal of Applied Mathematics and Mechanics* 59 (6) (1995) 853–863.

[18] D. Bernardo, M.I. Feigin, S.J. Hogan, M.E. Homer, Local analysis of C-bifurcations in N-dimensional piecewise-smooth dynamical systems, *Chaos, Solitons and Fractals* 10 (11) (1999) 1881–1908.

[19] D.T. Nguyen, S.T. Noah, C.F. Kettleborough, Impact behaviour of an oscillator with limiting stops, part I: a parametric study, *Journal of Sound and Vibration* 109 (2) (1986) 293–307.
[20] S. Natsiavas, H. Gonzalez, Vibration of harmonically excited oscillators with asymmetric constraints, *Journal of Applied Mechanics* 59 (1992) 284–290.
[21] S. Chatterjee, A.K. Mallik, Bifurcations and chaos in autonomous self-excited oscillators with impact damping, *Journal of Sound and Vibration* 191 (4) (1996) 539–562.
[22] G.W. Luo, J.H. Xie, Hopf bifurcation of a two-degree-of-freedom vibro-impact system, *Journal of Sound and Vibration* 213 (3) (1998) 391–408.
[23] G.W. Luo, J.H. Xie, Periodic motions and global bifurcations of a two-degree-of-freedom system with plastic impact, *Journal of Sound and Vibration* 240 (5) (2001) 387–858.
[24] G.W. Luo, Y.L. Zhang, J.N. Yu, Dynamical behavior of vibro-impact machinery near a point of codimension two bifurcation, *Journal of Sound and Vibration* 292 (1–2) (2006) 242–278.
[25] H.Y. Hu, Controlling chaos of a periodically forced nonsmooth mechanical system, *Acta Mechanica Sinica* 11 (3) (1995) 251–258.
[26] H.Y. Hu, Controlling chaos of a dynamical system with discontinuous vector field, *Physica D* 106 (1997) 1–8.
[27] J.P. Mejaard, A.D. De Pater, Railway vehicle systems dynamics and chaotic vibrations, *International Journal of Non-Linear Mechanics* 24 (1) (1989) 1–17.
[28] J. Zeng, S. Hu, Study on frictional impact and derailment for wheel and rail, *Journal of Vibration Engineering* 14 (1) (2001) 1–6.
[29] K. Yu, C.J. Luo Albert, The periodic impact responses and stability of a human body in a vehicle traveling on rough terrain, *Journal of Sound and Vibration* 272 (1–2) (2004) 267–286.
[30] L.A. Wood, K.P. Byrne, Analysis of a random repeated impact process, *Journal of Sound and Vibration* 78 (3) (1981) 329–345.
[31] Z.L. Huang, Z.H. Liu, W.Q. Zhu, Stationary response of multi-degree-of-freedom vibro-impact systems under white noise excitations, *Journal of Sound and Vibration* 275 (1–2) (2004) 223–240.
[32] Z.Z. Shu, X.Z. Shen, Theoretical analysis of complete stability and automatic vibration isolation of impacting and vibrating systems with double masses, *Chinese Journal of Mechanical Engineering* 26 (3) (1990) 50–57.
[33] J.E. Kozol, R.M. Brach, Two-dimensional vibratory impact and chaos, *Journal of Sound and Vibration* 148 (2) (1991) 319–327.
[34] J.H. Xie, The mathematical model for the impact hammer and global bifurcations, *Acta Mechanica Sinica* 29 (4) (1997) 456–463.
[35] J.M.T. Thompson, Complex dynamics of compliant offshore structures, *Proceedings of the Royal Society of London* A 387 (1983) 407–427.
[36] C.K. Sung, W.S. Yu, Dynamics of harmonically excited impact damper: bifurcations and chaotic motion, *Journal of Sound and Vibration* 158 (2) (1992) 317–329.
[37] P.R.S. Han, A.C.J. Luo, Chaotic motion of a horizontal impact pair, *Journal of Sound and Vibration* 181 (2) (1995) 231–250.
[38] M.S. Heiman, A.K. Bajaj, P.J. Sherman, Periodic motions and bifurcations in dynamics of an inclined impact pair, *Journal of Sound and Vibration* 124 (1) (1988) 55–78.
[39] C.N. Bapat, The general motion of an inclined impact damper with friction, *Journal of Sound and Vibration* 184 (3) (1995) 417–427.
[40] A. Kahraman, R. Singh, Non-linear dynamics of a geared rotor-bearing system with multiple clearances, *Journal of Sound and Vibration* 144 (3) (1991) 469–506.
[41] A. Kunert, F. Pfeiffer, Stochastic model for rattling in gear-boxes. in: W. Schiehlen (Ed.), *Nonlinear Dynamics in Engineering Systems*, Springer, Berlin, Heidelberg, 1990, pp. 173–180.
[42] H.J. Dong, Y.W. Shen, M.J. Liu, S.H. Zhang, Research on the dynamical behaviors of rattling in gear system, *Chinese Journal of Mechanical Engineering* 40 (1) (2004) 136–141.
[43] G. Iooss, J.E. Los, Quasi-genericity of bifurcation to high dimensional invariant tori for maps, *Communications in Mathematical Physics* 119 (1988) 453–500.
[44] V.I. Arnol'd, *Geometrical Methods in the Theory of Ordinary Differential Equations*, Springer, Berlin, 1983.
[45] D.K. Arrowsmith, C.M. Place, *An Introduction to Dynamical Systems*, Cambridge University Press, Cambridge, 1990.
[46] J. Guckenheimer, P.J. Holmes, *Nonlinear Oscillations, Dynamical Systems, and Bifurcations of Vector Fields*, second printing, Springer, New York, Berlin, Heidelberg, Tokyo, 1986.
[47] S. Wiggins, *An Introduction to Applied Nonlinear Dynamical Systems and Chaos*, Springer, Berlin, 1990.
[48] Y.A. Kuznetsov, *Elements of Applied Bifurcation Theory*, second ed., Springer, New York, 1998.
[49] Z.H. Ni, *Mechanical Vibration*, Xi'an Jiaotong University Press, 1989.
[50] J. Carr, *Applications of centre manifold theory, Applied Mathematical Sciences*, Vol. 35, Springer, Berlin, Heidelberg, New York, 1981.
[51] B.D. Hassard, N.D. Kazarinoff, Y.H. Wan, Theory and Applications of Hopf Bifurcation, London Mathematical Society Lecture Note Series, Vol. 41, 1981.
[52] O.E. Landford, *Bifurcation of Periodic Solution into Invariant Tori: The Work of Ruelle and Takrns, Lecture Notes in Mathematics*, Vol. 322, Springer, Berlin, 1973, pp. 159–192.
[53] R.J. Rogers, R.J. Pick, On the dynamic spatial response of a heat exchanger tube with intermittent baffle contacts, *Nuclear Engineering and Design* 36 (1976) 81–90.
[54] B.C. Wen, F.Q. Liu, *Theory and Application of Vibratory Mechanism*, Mechanism industry Press, Beijing, China, 1982.
[55] B.C. Wen, Y.L. Li, Q.K. Han, *Theory and Application of Nonlinear Oscillation*, Northeast University Press, Shenyang, China, 2001.